

CEACAM5 exacerbates asthma by inducing ferroptosis and autophagy in airway epithelial cells through the JAK/STAT6-dependent pathway

Si Liu*, Li Chen* and Yunxiao Shang

Department of Pediatrics, Shengjing Hospital of China Medical University, Shenyang, People's Republic of China

ABSTRACT

Objectives: Asthma, a prevalent chronic disease, poses significant health threats and burdens healthcare systems. This study focused on the role of bronchial epithelial cells in asthma pathophysiology.

Methods: Bioinformatics was used to identify key asthma-related genes. An ovalbumin-sensitized mouse model and an IL-13-stimulated Beas-2B cell model were established for further investigation.

Results: Carcinoembryonic antigen-related cell adhesion molecule 5 (CEACAM5) was identified as a crucial gene in asthma. CEACAM5 expression was elevated in asthmatic mouse lung tissues and IL-13-stimulated Beas-2B cells, primarily in bronchial epithelial cells. CEACAM5 induced reactive oxygen species (ROS), lipid peroxidation, and ferroptosis. Interfering with CEACAM5 reduced ROS, malondialdehyde levels, and enhanced antioxidant capacity, while inhibiting iron accumulation and autophagy. Overexpression of CEACAM5 in IL-13-stimulated cells activated the JAK/STAT6 pathway, which was necessary for CEACAM5-induced autophagy, ROS accumulation, lipid peroxidation, and ferroptosis.

Conclusion: CEACAM5 promotes ferroptosis and autophagy in airway epithelial cells via the JAK/STAT6 pathway, exacerbating asthma symptoms. It represents a potential target for clinical treatment.

KEYWORDS

Bronchial epithelial cells; CEACAM5; ferroptosis; autophagy; JAK; STAT6



Introduction

Asthma is a global chronic disease characterized primarily by chronic inflammation of the airways, variable airflow restriction, and high reactivity. This condition leads to recurrent symptoms such as wheezing, coughing, chest tightness, and shortness of breath, significantly impacting the quality of life of sufferers [1]. Asthma affects 300 million people globally, causing around 500,000 deaths annually and placing a heavy burden on healthcare systems due to treatment costs and disease management complexity [2]. Although low-dose inhaled corticosteroids and bronchodilators are usually effective for mild asthma patients, some severe asthma patients may require long-term reliance on oral corticosteroids [3]. This brings unavoidable side effects such as metabolic disorders, increased osteoporosis, and elevated risk of infections, limiting the sustainability and safety of treatment [4–6]. Furthermore, existing treatments primarily focus on controlling inflammation and alleviating symptoms, with insufficient exploration into the pathological mechanisms and discovery of new targets. Therefore, developing new therapeutic drugs and targeted therapies is a critical direction for current research.


Bronchial epithelial cells are the first line of defence in the respiratory tract and have been shown to be involved in various pathological changes associated with asthma, playing a significant role in the mechanisms of asthma onset [7,8]. Extensive research indicates that bronchial

epithelial cells influence the development and progression of asthma through their barrier function, immune modulation, inflammatory response, and airway remodeling [9]. In recent years, the study of ferroptosis in asthma has increasingly gained attention [10–12]. In bronchial epithelial cells of asthma patients, iron metabolism may be disrupted, leading to the accumulation of iron ions, which promotes lipid peroxidation and the production of lipid peroxides. This triggers oxidative stress, directly damaging cells and exacerbating inflammation, creating a vicious cycle [13–15]. Understanding the role of ferroptosis in asthma could aid in developing therapeutic strategies for this emerging field, potentially offering new means to treat asthma clinically. By regulating iron metabolism and alleviating oxidative stress, it may be possible to effectively control the pathological progression of asthma.

Ferroptosis is also associated with autophagic processes. Under asthmatic conditions, ferroptosis in bronchial epithelial cells could influence the autophagic pathway, altering the balance between cell survival and death [16]. Autophagy is a highly conserved intracellular degradation system that plays a crucial role in cell renewal and maintaining internal equilibrium [17]. Autophagy is involved in various cellular functions and plays a significant role in the pathophysiological mechanisms of many diseases [18, 19]. Studies have demonstrated a close relationship between autophagy and asthma, such as exacerbating airway inflammation and

CONTACT Yunxiao Shang  2018140134@cmu.edu.cn  Department of Pediatrics, Shengjing Hospital of China Medical University, Shenyang 110004, People's Republic of China

*These authors contributed equally to this work.

 Supplemental data for this article can be accessed online at <https://doi.org/10.1080/13510002.2024.2444755>.

© 2025 The Author(s). Published by Informa UK Limited, trading as Taylor & Francis Group

This is an Open Access article distributed under the terms of the Creative Commons Attribution-NonCommercial License (<http://creativecommons.org/licenses/by-nc/4.0/>), which permits unrestricted non-commercial use, distribution, and reproduction in any medium, provided the original work is properly cited. The terms on which this article has been published allow the posting of the Accepted Manuscript in a repository by the author(s) or with their consent.

airway remodeling [20]. Many autophagy-related genes have also been shown to participate in and regulate the onset and progression of asthma [21].

The JAK/STAT (Janus kinase/signal transducer and activator of transcription) pathway is a highly conserved signaling system in evolution, capable of regulating a variety of biological processes including inflammation, immune responses, embryonic development, cell division and proliferation, growth migration, and cell death, closely associated with immune diseases and cancer [22, 23]. In recent years, there has been an increasing amount of research linking the JAK/STAT pathway with autophagy and ferroptosis [24–26]. Activation of the IL-6/JAK/STAT3 pathway can enhance the level of autophagy in pancreatic cancer cells [24]. In *in vivo* and *in vitro* models of ischemia-reperfusion, activation of the JAK/STAT pathway can induce autophagy without affecting other kinase pathways, such as the MAPK and GSK-3 β pathways [25]. The activation of the JAK/STAT pathway is related to the production of inflammatory factors, which increase ROS generation and may accelerate ferroptosis in cells with abnormal iron levels. Additionally, the expression of genes related to iron metabolism, antioxidant defense, and lipid peroxidation (such as ferritin, hepcidin, and glutathione peroxidase) may be regulated by the JAK/STAT pathway [27]. IFN γ suppresses the expression of SLCA711 in adrenocortical carcinoma by increasing the activation of the JAK-STAT pathway, thus enhancing ferroptosis [28]. Activation of the JAK/STAT pathway could enhance the expression of inflammatory factors, further promoting the accumulation of iron ions and lipid peroxidation, thus exacerbating the occurrence of ferroptosis [27]. However, whether the JAK/STAT pathway can affect the progression of asthma by regulating autophagy and ferroptosis remains to be further studied.

CEACAM5 is a glycoprotein anchored to the cell membrane via a glycosylphosphatidylinositol linkage and belongs to the immunoglobulin superfamily and carcinoembryonic antigen family [29]. This protein is widely expressed on the surface of various cell types, including epithelial cells, endothelial cells, blood cells, and immune cells. CEACAM5 not only serves as an adhesion molecule but also has multiple biological functions, including regulating cell differentiation, immune responses, and inhibiting anoikis [30,31]. Studies have shown that the expression levels of CEACAM5 are elevated in induced sputum and serum samples of asthma patients and are associated with the patients' clinical symptoms, exhaled nitric oxide levels, and total serum IgE levels [32]. Furthermore, CEACAM5 is also highly expressed in the bronchial epithelial cells of asthma patients [33]. Despite this, research into the specific functions and mechanisms of action of CEACAM5 in asthma is still insufficient. Whether CEACAM5 can influence asthma through the regulation of ferroptosis and autophagy remains to be further investigated.

This study, through bioinformatics analysis, identified the key gene CEACAM5 in the bronchial epithelial cells of asthma patients and conducted research around the function and mechanism of CEACAM5 in asthma. By conducting both *in vivo* and *in vitro* experiments, the expression levels and localization of CEACAM5 were validated, and the study explored whether CEACAM5 regulated ferroptosis and autophagy in bronchial epithelial cells and its potential molecular mechanisms, providing feasible strategies for the treatment of asthma.

Materials and methods

Experimental animals and ethical statement

Female BALB/C mice, aged 6–8 weeks and weighing 18–22 g, free from specific pathogens (SPF), were purchased from Beijing Huafukang Bioscience Co., Ltd. All animal experiments were conducted at the SPF facility of the Benxi Experimental Base at China Medical University. The animal facility maintained a room temperature of 20–24°C, humidity between 50%–60%, and a 12-hour light/dark cycle. Mice had ad libitum access to food and water. Mice were acclimatized to these conditions for 7 days prior to any experimental manipulation. All animal husbandry and experimental procedures were carried out in strict accordance with ethical standards. This study was approved by the Animal Ethics Committee of China Medical University, with approval number 2022PS264 K.

Asthma mouse modeling and grouping

Twenty-four BALB/c mice were randomly divided into two groups (control group and asthma group), with 12 mice in each group. For the control group: on days 0, 7, and 14, the mice received an intraperitoneal injection of 200 μ L of saline. After 21 days, they were neutralized with saline (0.5 g ovalbumin, OVA + 10 mL saline) for 30 min once daily for one week. For the asthma group: on days 0, 7, and 14, the mice were given an intraperitoneal injection of 200 μ L of sensitizing solution (50 μ g OVA + 0.8 mg aluminium hydroxide gel + 130 μ L saline). After 21 days, they were neutralized with 5% OVA for 30 min once daily for one week. Mice were euthanized within 48 h after the last neutralization, and bronchoalveolar lavage fluid (BALF) and lung tissue samples were collected for subsequent experiments (Figure 1A).

Beas-2B cell culture and IL-13 treatment

The cells used in this experiment are Beas-2B human bronchial epithelial cell line, purchased from the Kunming Cell Bank of the Chinese Academy of Sciences. The Beas-2B cells were cultured in a serum-free medium specifically designed for them, supplemented with 10% fetal bovine serum (Sangon Biotech, Shanghai) and 1% penicillin-streptomycin solution (Transgene, Beijing).

IL-13 treatment. In this experiment, Beas-2B cells were treated with 20 ng/mL of IL-13 (Peprotech, USA) for 48 h to establish an asthma cell model. Once the cells reached 80% confluency and were in good growth condition, they were detached and counted. The cells were then seeded in a 6-well plate at approximately 4×10^5 cells per well, with 2 mL of medium added to each well before incubating for 24 h. For the control group, a medium exchange was performed, and for the IL-13 group, the medium containing 20 ng/mL IL-13 was added during the medium change. Cells were harvested after 48 h.

Cell transfection

The siRNA transfection was constructed by HeSheng Biotech, Beijing, with detailed sequence information available in Supplementary Table 1. The overexpression plasmid was also constructed by HeSheng Biotech, Beijing, inserting the CDS

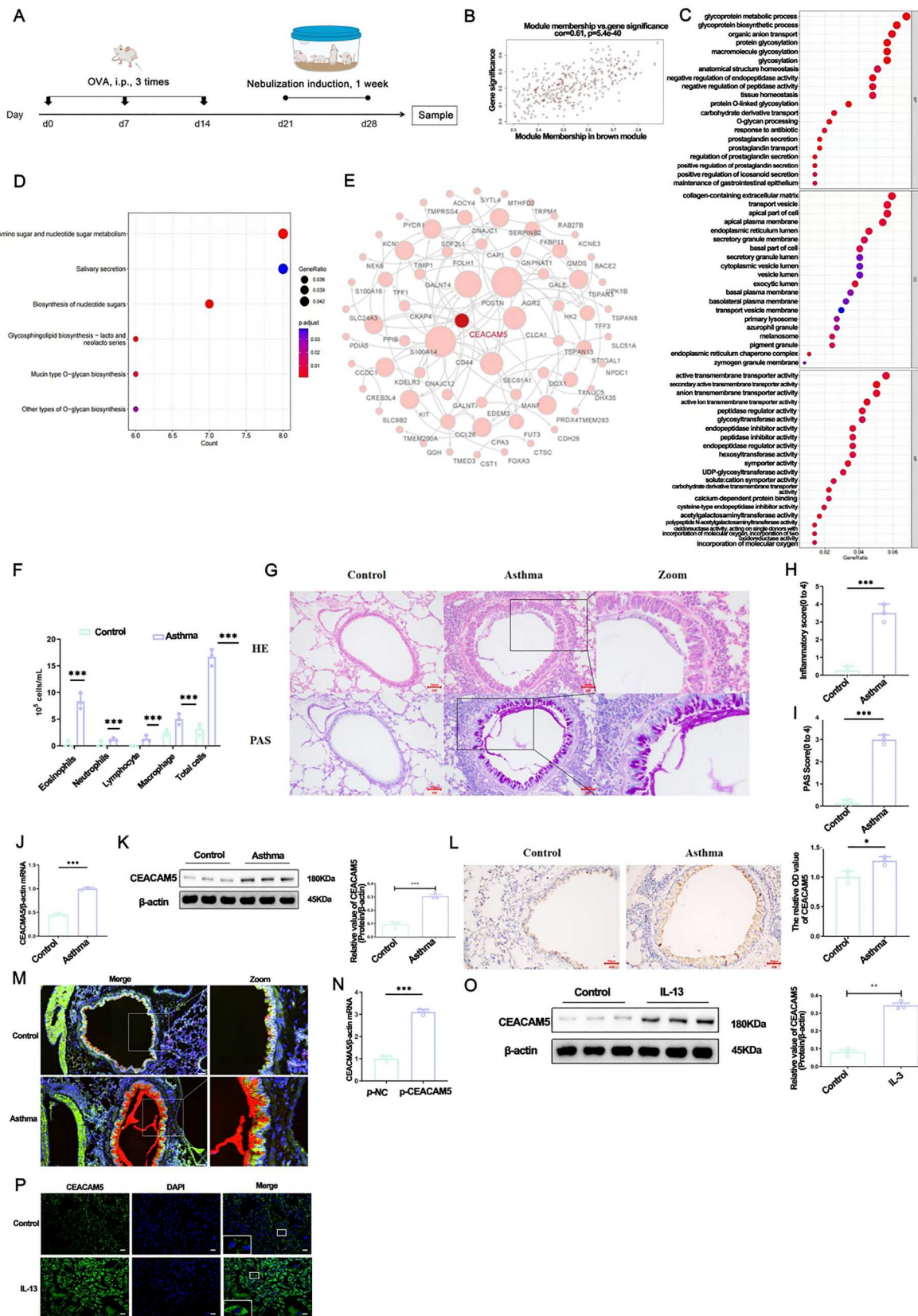


Figure 1. CEACAM5 is highly expressed in the asthma model. (A) Establishment of the asthma mouse model. (B) Relationship between brown module genes and gene significance. (C) Bubble plot of GO enrichment analysis of genes within the brown module, with MF, CC, and BF representing molecular function, biological process, and cellular component, respectively. (D) Bubble plot of KEGG pathway enrichment analysis. (E) PPI. (F) Total and classified counts of inflammatory cells in BALF. (G) HE and PAS staining of mouse lung tissue, 200 \times , scale bar 50 μ m, magnified view 400 \times . (H) Inflammatory cell infiltration score based on HE staining. (I) Quantification score based on PAS staining. (J) qPCR detection of CEACAM5 mRNA expression levels in mouse lung tissue. (K) Western blot detection of CEACAM5 protein expression levels in mouse lung tissue and statistical analysis of protein band grayscale values. (L) Immunohistochemical detection of CEACAM5 protein expression levels in mouse lung tissue, 200 \times , scale bar 50 μ m and semi-quantitative analysis. (M) Immunofluorescence detection of CEACAM5 protein expression in mouse lung tissue, 200 \times , scale bar 50 μ m, red fluorescence represents CEACAM5, green fluorescence represents E-cadherin, blue fluorescence represents nuclei. (N) qPCR detection of CEACAM5 mRNA expression levels in Beas-2B cells. (O) Western blot detection of CEACAM5 protein expression levels in Beas-2B cells and statistical analysis. (P) Immunofluorescence staining showing CEACAM5 expression in Beas-2B cells, 400 \times , scale bar 50 μ m, green fluorescence represents CEACAM5, blue fluorescence represents nuclei. Values are expressed as mean \pm standard deviation, $n = 3$ or 12; * $P < 0.05$, ** $P < 0.01$, *** $P < 0.001$ compared with the control group.

region of the human CEACAM5 gene (transcript number: NM_004363.6) into the pcDNA3.1 vector (p-CEACAM5), with the pcDNA3.1 empty vector (p-NC) serving as the negative control.

Transfection was carried out when the Beas-2B cells reached 80% confluency. According to the recommended dosage from the Lipofectamine3000 (Invitrogen, USA) manual, siRNA or plasmid was diluted in opti-MEM medium (Gibco, USA) (plasmid dilution required the addition of P3000, siRNA did not), to prepare solution I. Opti-MEM medium was used to dilute Lipofectamine3000, to prepare solution II. Solutions I and II were mixed thoroughly and left at room temperature for 20 min. According to the recommended volume, the mixture was added to the wells of the cell plate, shaken to mix, and then incubated in the cell culture incubator. The medium was changed after 24 h.

Based on whether siRNA transfection and IL-13 treatment were performed, the groups were divided into: si-NC group (transfected with negative control siRNA, no IL-13 treatment), si-CEACAM5 group (transfected with siRNA targeting human CEACAM5, no IL-13 treatment), si-NC + IL-13 group (transfected with negative control siRNA, then given IL-13 treatment), and si-CEACAM5 + IL-13 group (transfected with siRNA targeting human CEACAM5, then given IL-13 treatment).

Based on whether plasmid transfection and IL-13 treatment were performed, the groups were divided into: p-NC group (transfected with negative control plasmid, no IL-13 treatment), p-CEACAM5 group (transfected with CEACAM5 overexpression plasmid, no IL-13 treatment), p-NC + IL-13 group (transfected with negative control plasmid, then given IL-13 treatment), and p-CEACAM5 + IL-13 group (transfected with CEACAM5 overexpression plasmid, then given IL-13 treatment).

Mice adenovirus (AAV)- CEACAM5 Transfection

To investigate the effects of interference with CEACAM5 on asthma, an off-the-shelf AAV vector (AAV-shCEACAM5) was used. The mice were injected with intrabronchial AAV under anesthesia, and each mouse was injected with 10 μ L of disease venom with a concentration of 1×10^{12} vg/mL. The control group was injected with AAV containing negative control sequences. 2–4 weeks after injection, mice were killed, lung tissues were extracted for RNA, and the mRNA expression of CEACAM5 was analyzed by qPCR, while the protein level was detected by Western blot.

AG490 blocking experiment

For the JAK pathway inhibitor AG490 (MCE, Shanghai) experiment, cells were divided into four groups: p-NC group, p-CEACAM5 group, p-NC + AG490 group, and p-CEACAM5 + AG490 group. The concentration of AG490 used was 10 μ M, with a treatment duration of 2 h, after which all four groups of cells were treated with 20 ng/mL IL-13 for 48 h [34].

CEACAM5 expression analysis in asthma model database

To investigate the expression of CEACAM5 in asthma, a search was conducted in the Gene Expression Omnibus (GEO) database. The search terms used were ‘asthma’ and the species

was limited to ‘Homo sapiens’, with the study type restricted to ‘Expression profiling by array’ to retrieve gene expression microarray datasets that meet the following criteria: (1) Data from expression profiling microarrays; (2) The specimens submitted were human bronchial epithelial cells obtained via bronchoscopic brushing; (3) There were no duplicate samples within the datasets. Based on these criteria, three datasets were ultimately selected for inclusion in this study: GSE67472 (including 62 patients with mild to moderate asthma and 43 healthy controls) [35], GSE63142 (including 72 patients with mild to moderate asthma, 56 with severe asthma, and 27 healthy controls) [36], and GSE43696 (including 50 patients with mild to moderate asthma, 38 with severe asthma, and 20 healthy controls) [37].

The datasets GSE67472, GSE63142, and GSE43696 were downloaded from the GEO database. Using platform information, probe names were annotated to gene names; when duplicate gene names appeared, averages were taken to remove duplicates, and then datasets were merged. Batch normalization was applied using the ComBat function from the ‘sva’ package in R to eliminate batch effects between different samples, and box plots and Principal Component Analysis (PCA) charts of sample gene expression levels before and after removing batch effects were produced to verify the effectiveness of batch correction. The Median Absolute Deviation method was used to select the top 5000 genes for further data analysis.

Weighted Gene Co-expression Network Analysis (WGCNA) delineates patterns of gene association between different samples, identifying highly co-varying gene sets, and identifies candidate biomarkers or therapeutic targets based on the connectivity within the gene set and its association with phenotypes. Gene co-expression network analysis is conducted using the ‘WGCNA’ package in R. The pickSoft-Threshold function is used to select an appropriate soft threshold β to achieve an R-squared of 0.85, at which point the connections between genes in the gene network follow a scale-free network distribution. Based on the determined soft threshold, a gene co-expression network is established to classify genes into different modules. The gene co-expression matrix is transformed using the soft threshold to create an adjacency matrix, and on this basis, a topological overlap matrix (TOM) is constructed, identifying different gene modules and the number of genes each module contains. The module eigengene (ME) is the first principal component gene (eigengene) of a module and best represents the gene expression profile within that module. Using the ME, the correlations between modules can be ascertained, and combining ME with phenotype data allows for the identification of the module’s correlation with phenotypes, thereby selecting disease-related modules of interest for further analysis.

Modules of interest contain many genes, and core genes within these modules exhibit a high Module Membership (MM). MM represents the correlation coefficient between a gene and the module eigengene, indicating the gene’s affiliation within the module. Furthermore, hub genes should have significant relevance to clinical features. The significance of these genes in relation to clinical features should be calculated based on the type of clinical data available (using correlation coefficients for continuous data and methods such as t-tests for categorical data) to determine significant *P*-values. These are then log-transformed using base 10 to quantify

the correlation between genes and clinical features, termed Gene Significance (GS). Hub genes are selected based on these two characteristics. In this study, genes are defined as hub genes if they simultaneously meet the criteria of $MM > 0.8$ and $GS > 0.4$ with clinical features.

GO, KEGG, and PPI analysis

To further explore the functions of hub genes, we conducted Gene Ontology (GO) and Kyoto Encyclopedia of Genes and Genomes (KEGG) enrichment analysis. This study utilized the clusterProfiler package in R for both GO and KEGG enrichment analysis.

To generate a Protein-Protein Interaction (PPI) network diagram, genes from the Brown module with $MM > 0.6$ and $GS > 0.2$ were uploaded to the '<https://string-db.org/>' website to construct the gene's protein interaction network relationships, with the minimum required interaction score set at 0.400. The resultant PPI network interactions were then imported into Cytoscape 3.8.2 (Cytoscape Consortium). Using the built-in analysis functions of the software, genes were sorted by their Degree values, and colors were customized according to gene names.

Bronchoalveolar lavage fluid (BALF) collection and inflammatory cell analysis

The lungs were lavaged with saline, and the lavage fluid was centrifuged at 4°C and 1500 rpm for 10 min. The supernatant was stored at a low temperature, and the sediment was re-suspended in 0.5 mL of phosphate-buffered saline. A haemocytometre was used to count the number of cells in 1 mL of BALF. Specifically, 0.1 mL of the resuspended BALF was placed onto a slide and smeared. After air-drying, the slide was fixed with methanol for 10 min and then air-dried again before being placed in a humid chamber. Giemsa stain (Beyotime, shanghai) was added to cover the entire smear and left for 2 min. Giemsa A solution was then applied to the appropriate areas of the slide for 1.5 min. After adding phosphate-buffered saline, the slide was gently shaken to mix well with the Giemsa staining solution. After 5 min, the staining solution was washed off with PBS. The slide was air-dried and then examined under a microscope for cell differentiation and counting.

Preparation of lung tissue paraffin sections and hematoxylin-eosin (HE) staining

The right lung of the mouse was isolated and fixed in 4% paraformaldehyde for 48 h. The lung tissue was dehydrated sequentially in 75% ethanol, 85% ethanol, 90% ethanol, 95% ethanol, and 100% ethanol; cleared in xylene; and thoroughly immersed in melted paraffin, then embedded in paraffin and solidified.

The tissue was sectioned into 3 μm thick slices. The sections were stained with hematoxylin (Beyotime, shanghai) for 2 min, blued under running tap water, and then stained in eosin (Beyotime, shanghai) for 1 min. Lung tissue pathological changes were observed under a microscope. To quantitatively score the HE-stained lung tissue sections, a score of 0 was given for no inflammatory cell infiltration around the airways; a score of 1 for a small amount of inflammatory cells; a score of 2 for a single layer of inflammatory cells; a score of 3 for infiltration of

2–4 layers of inflammatory cells; and a score of 4 for more than 4 layers of inflammatory cell infiltration.

Periodic acid-schiff (PAS) staining

Lung tissue paraffin sections were dewaxed in xylene and rehydrated in ethanol solution of ascending concentrations. Periodic acid solution (Beyotime, shanghai) was then applied to the sections for 8 min to perform periodic acid oxidation, followed by a 5-minute soak in PBS for washing. Schiff's reagent was added for Schiff staining for 20 min. The sections were then washed in PBS for another 5 min; hematoxylin was applied to stain the nuclei for 2 min, followed by differentiation in differentiation solution for 10 s, and then blued under running water. The sections were dehydrated in descending concentrations of ethanol, cleared in xylene, and mounted in neutral gum.

Under the microscope, PAS-stained sections were quantitatively scored based on the intensity of magenta staining of the airway epithelium, indicative of high mucous secretion. A score of 0 was given if there was no magenta staining of the airway epithelium; a score of 1 if less than 25% of the cells were stained; a score of 2 if 25–50% of the cells were stained; a score of 3 if 50–75% of the cells were stained; and a score of 4 if more than 75% of the cells were stained.

Western blotting

Mouse lung tissues were treated with RIPA lysis buffer (Biosharp, Anhui) containing PMSF (Biosharp, Anhui) and phosphatase inhibitors, and proteins were extracted via ultrasonic disruption and low-temperature high-speed centrifugation. Protein concentrations were determined using a BCA assay kit (Biosharp, Anhui), with concentrations calculated against a standard curve. Protein samples were mixed with protein loading buffer and denatured by heating, then cooled and stored at low temperatures for subsequent experiments. A 5% stacking gel and 15%/12% resolving polyacrylamide gels were prepared, and equal amounts of protein samples were subjected to SDS-PAGE until complete separation of proteins was achieved. A transfer sandwich was prepared and assembled for the transfer of target proteins to a PVDF membrane. The PVDF membrane was blocked with 5% skimmed milk, followed by incubation with primary and secondary antibodies. Protein bands were visualized using ECL detection reagent (Vazyme, Nanjing). Subsequent densitometric analysis was conducted to quantify protein expression levels. Details of the antibodies are provided in Supplementary Table 2.

Real-Time fluorescent quantitative PCR

A total of 20–40 mg of frozen mouse lung tissue was thoroughly lysed in Trizol (TransGene, Beijing), followed by the addition of chloroform for phase separation. The mixture was then centrifuged at low temperature and high speed to separate and extract the RNA from the supernatant. An equal volume of isopropanol was added and left to stand at low temperature to precipitate the RNA, which was subsequently purified through washing, centrifugation, and drying steps, and resuspended in DEPC water for further experiments or storage in a freezer. The concentration of RNA was measured using a NanoDrop 2000/2000C spectrophotometer.

Following the instructions of the reverse transcription kit (Takara, Dalian), to remove genomic DNA from mouse lung tissue RNA, RNA samples diluted to 500 µg/ml were mixed with a specialized reaction mixture and incubated in a PCR machine at 42°C for 2 min. Next, the reverse transcription mix was added to the treated RNA samples and reacted in the PCR machine at 37°C for 15 min, followed by 85°C for 5 s to prepare the cDNA. Finally, the diluted primers and cDNA were used to prepare the RT-PCR amplification reaction system, which was then amplified on an Applied Biosystems 7500 machine, and the results were analyzed post-amplification. Detailed qRT-PCR sequence information is provided in Supplementary Table 3.

Immunofluorescence

Immunofluorescence double staining was used to detect the expression of CEACAM5 in the airway epithelium of asthmatic mice or cell models. Paraffin sections of lung tissue were dewaxed to water, and antigen retrieval was performed in citrate antigen retrieval buffer (Beyotime, Shanghai), followed by blocking in 5% BSA at 37°C for 30 min. Primary antibodies (CEACAM5, rabbit-derived, 1:100; E-cadherin, mouse-derived, 1:100) were added to the sections and incubated overnight at 4°C. After washing three times with PBS, secondary antibodies (CY3-labelled and FITC-labelled) were added and incubated for 60 min at room temperature in the dark. After three washes with PBS, the sections were stained with DAPI (Beyotime, Shanghai) at room temperature for 5 min and then mounted using an anti-fade mounting medium. The pathological slides were observed under a fluorescence microscope (Eclipse Ti2, Nikon, Japan). For cell samples, cell smears were prepared, fixed in 4% paraformaldehyde for 20 min, and permeabilised with 0.1% Triton to cover the cells. This was followed by blocking, antibody incubation, nuclear staining, and mounting.

Construction of a stable cell line with autophagy dual reporter lentivirus (mRFP-GFP-LC3)

When the Beas-2B cells reached 80% confluence, the medium was replaced with fresh culture medium, and polybrene and mRFP-GFP-LC3 virus solution at 20 MOI (Hanheng Biotech, China) were sequentially added and mixed well. After 24 h of transfection, the medium was replaced with fresh culture medium. After 48 h, the GFP/RFP expression efficiency was analyzed using a fluorescence microscope. Once the cell growth was stable, the cell line was selected with culture medium containing 1 µg/ml puromycin. Under a fluorescence microscope, most cells showed distinct green fluorescence spots at 488 nm wavelength and distinct red fluorescence spots at 560 nm wavelength, indicating successful selection and the establishment of a stable Beas-2B cell line expressing mRFP-GFP-LC3.

Autophagy flux assay

Using the stable mRFP-GFP-LC3-Beas-2B cell line, the cell culture and cell smear procedures were as previously described, with cells subjected to different conditions based on experimental grouping. After fixing and mounting the cells, they were observed under a confocal fluorescence microscope, and the number of fluorescence spots was counted. In the green fluorescence channel images, green spots represent autophagosomes; in the red fluorescence

channel images, red spots represent autolysosomes; in the merged images, yellow spots represent autophagosomes, and red spots represent autolysosomes.

Immunohistochemistry

Following the instructions provided with the immunohistochemistry kit (Elabscience, China), lung tissue sections were dewaxed and boiled in antigen retrieval solution for 10 min, treated with 3% hydrogen peroxide for 30 min to inactivate endogenous peroxidases, and blocked with serum for 30 min. The sections were incubated overnight at 4°C with a rabbit anti-CEACAM5 polyclonal antibody (Affinity, USA, diluted 1:200). This was followed by a 30-minute room temperature incubation with HRP-labelled goat anti-rabbit IgG (Proteintech, Wuhan, China). The lung tissues were stained using DAB chromogen, counterstained with hematoxylin, and blued under running water. The sections were dehydrated sequentially in ethanol and xylene and mounted with neutral gum. Observations and photography were performed under a microscope. The average optical density (OD) of immunohistochemical positive staining was quantified using ImageJ 1.8.0 (National Institutes of Health), with the results presented in bar charts.

2',7'-Dichlorodihydrofluorescein Diacetate (DCFH-DA) staining

Fresh mouse lung tissue was immersed in OCT compound and sectioned into 10-micron thick slices using a cryostat (Leica, USA). To detect the levels of reactive oxygen species (ROS) in the tissue, according to the guidelines of the DCFH-DA assay kit, the tissue sections were incubated in the dark at 37°C with a 10 µM concentration of DCFH-D fluorescent probe for 30 min. Subsequently, green fluorescence signals were observed using a confocal fluorescence microscope from Olympus (Tokyo).

Seahorse assay

Oxygen consumption rates were measured using seahorse XF extracellular flux Analyzer (Agilent Technologies). The cells were inoculated into the seahorse XF assay plate at a density of approximately 10,000 cells per well. Then incubate at 37°C for 1 h. According to the manufacturer's instructions, compounds including oligomycin A (1 µM), FCCP (1 µM) and antimycin A (0.5 µM) were continuously injected on microplates and oxygen consumption rates were measured in real time using a mitochondrial stress test kit.

Biochemical assays

In a low-temperature environment, freshly collected mouse lung tissue was mixed with saline in a 1:9 ratio and homogenized using a high-throughput tissue grinder. After homogenization, the tissue was centrifuged at low speed to remove all tissue sediments, and the supernatant was collected. According to the manual provided with the kit (Nanjing Jiancheng Bioengineering Institute, Nanjing, China), the obtained supernatant was further analyzed using biochemical assay kits. The absorbance was measured at wavelengths of 532, 240, 340, 420, and 520 nm to quantitatively analyze malondialdehyde (MDA), catalase (CAT), reduced glutathione (GSH)/ oxidized glutathione (GSSG), and total antioxidant capacity (T-AOC),

respectively. By calculating the content or activity of each indicator using the relevant formulas, the redox status in the tissue was assessed.

Iron content

Following the instructions of the Tissue Iron (Fe) Assay Kit (Nanjing Jiancheng), a standard curve was prepared using iron standards, and the homogenate of freshly collected lung tissue was measured. The absorbance was measured at a wavelength of 520 nm to calculate the iron content in the tissue.

TEM observation

Fresh mouse lung tissue or Beas-2B cells were collected and fixed for 2 h at 4°C in 2.5% glutaraldehyde fixative (pH = 7.3). The samples were then washed multiple times with PBS to remove any residues. Subsequently, the samples were immersed in 1% osmium tetroxide in the dark at room temperature for 7 h. After this, the samples were dehydrated through a series of acetone solutions at 50, 70, 90, and 100% concentrations, infiltrated in resin, and polymerized at high temperature. The sections were then stained in the dark for 8 min using a 2% uranyl acetate saturated alcohol solution. The sections were placed in a copper grid box to dry overnight at room temperature. The lung tissue's microstructure was observed under a transmission electron microscope.

Statistical analysis

Statistical analysis and graphing were performed using GraphPad Prism 8 (GraphPad Software, Inc.). Quantitative data are presented as mean \pm standard deviation. Comparisons between two groups were conducted using the t-test, while comparisons among multiple groups were made using one-way analysis of variance (One-way ANOVA). A P value < 0.05 was considered statistically significant.

Results

CEACAM5 is highly expressed in asthma

Initially, three datasets from the GEO database that met the criteria – GSE67472, GSE63142, GSE43696 – were merged and batch-corrected (Supplementary Figure 1). The merged dataset included 368 samples and 16,174 genes. The top 5000 genes, selected based on median absolute deviation, were used for further analysis. After removing batch effects, gene expression data from the 368 samples were used to construct a sample hierarchical clustering tree and clinical information relationship diagram. A β value of 7 was chosen to construct the gene co-expression network, at which the fit coefficient R^2 (SFT.R.sq) was 0.90. Under this parameter, the average connectivity of each gene module was 69.71, with a median of 63.08 and a maximum connectivity of 193.51 (Supplementary Figure 2 and Supplementary Table 4). Subsequently, hierarchical clustering based on adjacency value differences resulted in a gene clustering tree, identifying 15 gene modules (Supplementary Figure 3 and Supplementary Table 5). Cluster analysis of module eigengenes was conducted, and Pearson correlation coefficients were calculated between them, linking module eigengenes with sample

grouping (healthy vs. asthma), identifying 379 genes strongly positively correlated with asthma (Supplementary Figure 4). Figure 1B shows a scatter plot of Module Membership (MM) and Gene Significance (GS) for genes in the Brown module. By setting $MM > 0.8$ and $GS > 0.4$, one hub gene was identified in the Brown module: CEACAM5, which was selected as the hub gene for subsequent experimental analysis in this study (Figure 1B).

To further investigate the gene functions within the Brown module, we conducted GO and KEGG enrichment analyses on the 379 genes from the Brown module and created a PPI protein interaction network diagram. The GO functional analysis revealed that the genes in the Brown module play roles in maintaining tissue homeostasis and anatomical structure stability (Figure 1C). KEGG analysis indicated that these genes are primarily involved in the metabolism of amino sugars and nucleotide sugars, as well as the biosynthesis of nucleotide sugars (Figure 1D). Genes in the Brown module with $MM > 0.6$ and $GS > 0.2$ were used to construct a PPI, showing CEACAM5 in a relatively central position interacting with various proteins (Figure 1E, with CEACAM5 represented by red dots). Oxidative stress, ferroptosis, and cellular autophagy are closely related to the maintenance of cell and tissue homeostasis. Based on the results of these enrichment analyses, we hypothesize that these genes may be involved in the aforementioned processes.

Subsequently, we established an *in vivo* model of asthma in mice. The results revealed that the total number of inflammatory cells, eosinophils, neutrophils, lymphocytes, and mononuclear macrophages in the BALF of the asthma group was significantly higher than that of the control group ($P < 0.001$, Figure 1F). This was primarily characterized by an increase in eosinophils. These results indicate that there was an increase in airway inflammation in the mice of the asthma group, and the asthma model represented eosinophilic asthma. The results of HE and PAS staining showed that there was a significant increase in inflammatory cell infiltration around the bronchi and blood vessels in the lung tissue of the asthma group, with deformities in the bronchial epithelium, hypertrophic proliferation, thickening of the bronchial walls, secretion of mucus within the lumen, and thickening of the smooth muscle. In contrast, the lung tissue of the control group showed no significant infiltration of inflammatory cells around the bronchi and blood vessels, and the bronchial epithelium was intact. PAS staining for glycogen allowed observation of mucus secretion by airway epithelial cells, with a marked increase in PAS-positive cells in the asthma group compared to the control group, indicating a high secretion of mucus in the airways of the asthma group. The scores for inflammatory cell infiltration and PAS staining were significantly higher in the asthma group than in the control group ($P < 0.001$, Figure 1G–I).

Then, the expression levels of the key gene CEACAM5 screened for inflammation in mouse lung tissues were examined. The results showed that both the mRNA level and protein expression level of CEACAM5 were significantly higher than those in the control group ($P < 0.001$ or $P < 0.01$), suggesting an increased expression of CEACAM5 in the lung tissues of asthmatic mice (Figure 1J–K). Furthermore, immunohistochemical staining of lung tissue sections showed that CEACAM5 was mainly expressed in bronchial epithelial cells, with significantly higher expression of CEACAM5 in the airway epithelial cells of asthmatic mice

compared to the control group ($P < 0.01$, Figure 1L). Immunofluorescent double staining of lung tissue sections for CEACAM5 (red fluorescence) and E-cadherin (green fluorescence) clearly showed that E-cadherin green fluorescence was expressed in various epithelial cells, while CEACAM5 red fluorescence was mainly expressed in airway epithelium, and compared to the control group, the expression of CEACAM5 in the asthmatic group was significantly increased (Figure 1M).

IL-13 stimulation of Beas-2B cells resulted in a significant increase in p-STAT6 protein expression levels compared to the control group ($P < 0.001$), demonstrating the biological activity of IL-13 and the successful establishment of an in vitro asthma model (Figure S5A–B). The mRNA and protein expression levels of CEACAM5 were both significantly higher than those in the control group ($P < 0.001$ or $P < 0.01$, Figure 1N–O). Immunofluorescence staining of cells revealed that CEACAM5 was mainly expressed in the cell membrane and cytoplasm. The

fluorescence signal of CEACAM5 in the control group was weak, while after IL-13 treatment, the fluorescence intensity of CEACAM5 significantly increased (Figure 1P), indicating high expression of CEACAM5 in IL-13-stimulated Beas-2B cells.

CEACAM5 induces ROS accumulation and lipid peroxidation in lung tissues of asthmatic mice and human bronchial epithelial cells

The lungs are one of the organs susceptible to the influence of ROS, with their damage often associated with oxidative stress. DCFH-DA serves as a fluorescent probe capable of detecting intracellular ROS. Therefore, in this study, DCFH-DA staining technique was employed to assess the ROS levels in frozen sections of lung tissues from asthmatic mice. The research findings revealed enhanced ROS signals in the lung tissues of asthmatic experimental group mice compared to those in the control group (Figure 2A). At the

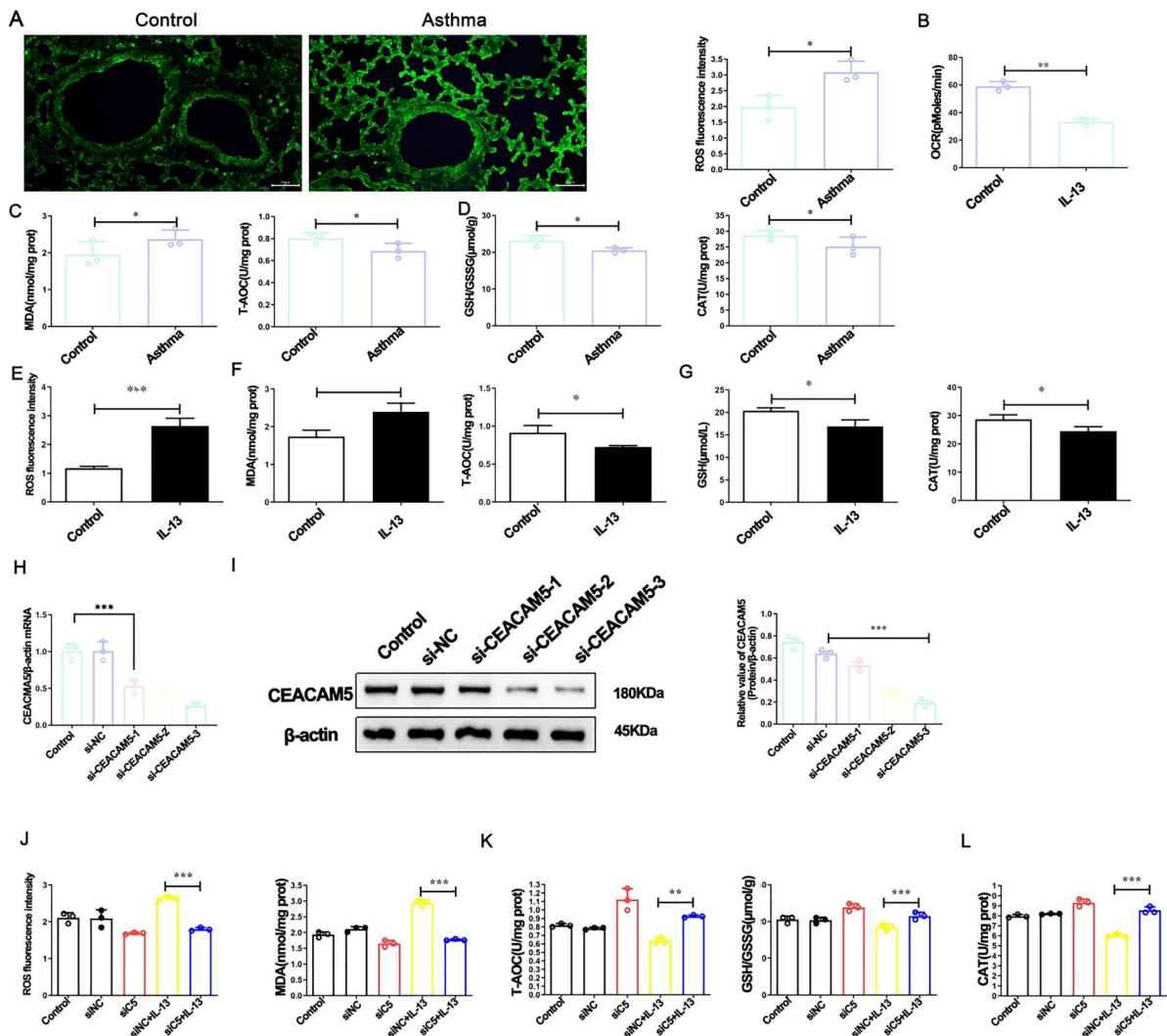


Figure 2. CEACAM5 induces ROS accumulation and lipid peroxidation in lung tissues of asthmatic mice and human bronchial epithelial cells. Mice and Beas-2B cells were divided into control and asthma groups. (A) DCFH-DA staining analysis of ROS levels in frozen sections of mouse lung tissues. (B) The effects of OCR on Beas-2B cells were measured using Seahorse XF extracellular flux analyzer. (C) Biochemical detection of MDA and T-AOC levels in lung tissue homogenate of mice. (D) Biochemical detection of GSH/GSSG ratio and CAT enzyme activities in lung tissue homogenate of mice. (E) DCFH-DA staining analysis of ROS levels in IL-13-stimulated Beas-2B cells. (F) Biochemical detection of MDA and T-AOC levels in supernatant of Beas-2B cells. (G) Biochemical detection of GSH/GSSG ratio and CAT enzyme activities in supernatant of Beas-2B cells. IL-13-stimulated Beas-2B cells were divided into blank cell control group, siNC control group, and si-CEACAM5-1/2/3 interference group. (H) qPCR analysis of CEACAM5 interference efficiency in Beas-2B cells. (I) Western blot detection of CEACAM5 interference efficiency in Beas-2B cells. IL-13-stimulated Beas-2B cells were divided into si-NC group, si-CEACAM5 group, si-NC + IL-13 group, and si-CEACAM5 + IL-13 group. (J) DCFH-DA staining analysis of ROS levels in Beas-2B cells after CEACAM5 interference. (K) Biochemical detection of MDA and T-AOC levels in Beas-2B cells after CEACAM5 interference. (L) Biochemical detection of GSH/GSSG ratio and CAT enzyme activities in Beas-2B cells after CEACAM5 interference. Values are expressed as mean \pm standard deviation, $n = 3$; * $P < 0.05$, ** $P < 0.01$, *** $P < 0.001$ compared with the control group.

same time, mitochondrial OCR in Beas-2B cells was measured by Seahorse XFe24 extracellular flux analyzer, and the results showed that the OCR in Beas-2B cells after IL-13 treatment was reduced compared to the control group (Figure 2B). Biochemical assays showed increased MDA content and decreased T-AOC in the lung tissue homogenate of asthmatic experimental group mice, along with reduced GSH/GSSG ratio and CAT enzyme activities (Figure 2C–D). Similar results were further validated in IL-13-stimulated Beas-2B cells (Figure 2E–G), indicating that asthma induces ROS accumulation and oxidative stress damage in lung tissues and Beas-2B cells.

To further validate the role of CEACAM5 in asthma-induced respiratory oxidative stress damage, this study used IL-13-stimulated Beas-2B cells as an in vitro model and performed interference on the CEACAM5 gene. Firstly, qPCR was used to compare the interference efficiency of different si-CEACAM5 in Beas-2B cells, with si-CEACAM5-3 showing the most significant inhibition of gene transcription and protein expression levels (Figure 2H–I). DCFH-DA staining results demonstrated a significant reduction in ROS levels in

Beas-2B cells after CEACAM5 interference (Figure 2J), along with decreased MDA content, increased T-AOC content, and enhanced GSH/GSSG ratio and CAT enzyme activities (Figure 2K–L). These results suggest that inhibiting CEACAM5 expression can alleviate asthma-induced oxidative stress.

CEACAM5 induces ferroptosis in lung tissues of asthmatic mice and human bronchial epithelial cells

Oxidative stress increases the production of reactive oxygen species, indirectly triggering ferroptosis, a iron-dependent form of cell death. In this study, we found that compared to the control group mice, the lung tissue homogenate of asthmatic mice showed increased iron content (Figure 3A). The expression of ferritin light chain (FTL), a protein involved in regulating cellular iron ion storage and balance, was decreased, while the expression of NCOA4 and 4-HNE, which mediates the degradation of iron proteins and releases iron ions, was increased. Additionally, the expression of GPX4, and xCT, which are involved in antioxidant defence against

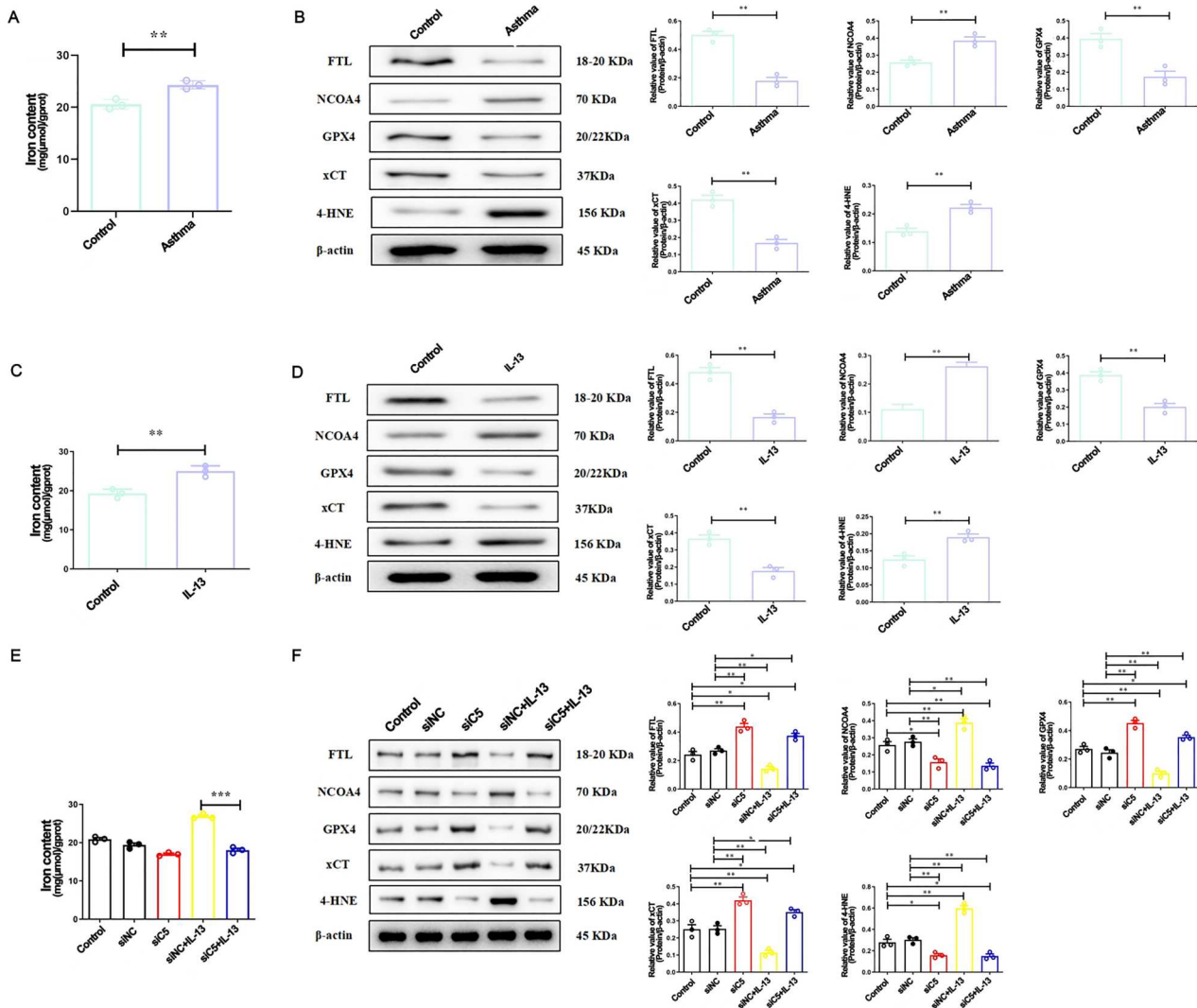


Figure 3. CEACAM5 induces ferroptosis in lung tissues of asthmatic mice and human bronchial epithelial cells. Mice and Beas-2B cells were divided into control and asthma groups. (A) Biochemical detection of iron content in lung tissue homogenate of asthmatic mice. (B) Western blot detection of FTL, NCOA4, GPX4, xCT, and 4-HNE protein expression in lung tissue of asthmatic mice. (C) Biochemical detection of iron content in IL-13-stimulated Beas-2B cells. (D) Western blot detection of FTL, NCOA4, GPX4, xCT and 4-HNE protein expression in IL-13-stimulated Beas-2B cells. IL-13-stimulated Beas-2B cells were divided into si-NC group, si-CEACAM5 group, si-NC + IL-13 group, and si-CEACAM5 + IL-13 group. (E) Biochemical detection of iron content in Beas-2B cells after interference of CEACAM5. (F) Western blot detection of FTL, NCOA4, GPX4, xCT, and 4-HNE protein expression in Beas-2B cells after interference of CEACAM5. Values are expressed as mean ± standard deviation, n = 3; *P < 0.05, **P < 0.01, ***P < 0.001 compared with the control group.

lipid peroxidation, was decreased (Figure 3B). Similar results were further validated in IL-13-stimulated Beas-2B cells (Figure 3C–D). The changes in protein expression regulating ferroptosis indicate that oxidative stress induced by asthma mediates ferroptosis.

To further validate the role of CEACAM5 in asthma-induced respiratory ferroptosis, this study employed IL-13-stimulated Beas-2B cells as an in vitro model and performed interference on the CEACAM5 gene. The results of iron content detection showed a significant decrease in iron content in Beas-2B cells after CEACAM5 interference (Figure 3E). The expression levels of ferritin light chain (FTL) increased, while the protein expression levels of NCOA4 and 4-HNE decreased. Moreover, the inhibition of GPX4 and xCT proteins was alleviated (Figure 3F). These results indicate

that inhibiting CEACAM5 expression can alleviate asthma-induced ferroptosis.

CEACAM5 induces autophagy in lung tissues of asthmatic mice and human bronchial epithelial cells

The formation of autophagosomes or autolysosomes observed under transmission electron microscopy is direct evidence of autophagy occurrence. In this experiment, transmission electron microscopy was used to observe autophagic phenomena in airway epithelial cells of mouse lung tissue specimens. The results showed (Figure 4A) the presence of autophagosomes (red dotted circles) with double-membrane structures, enclosing cytoplasmic components or organelles, and autolysosomes (yellow dotted

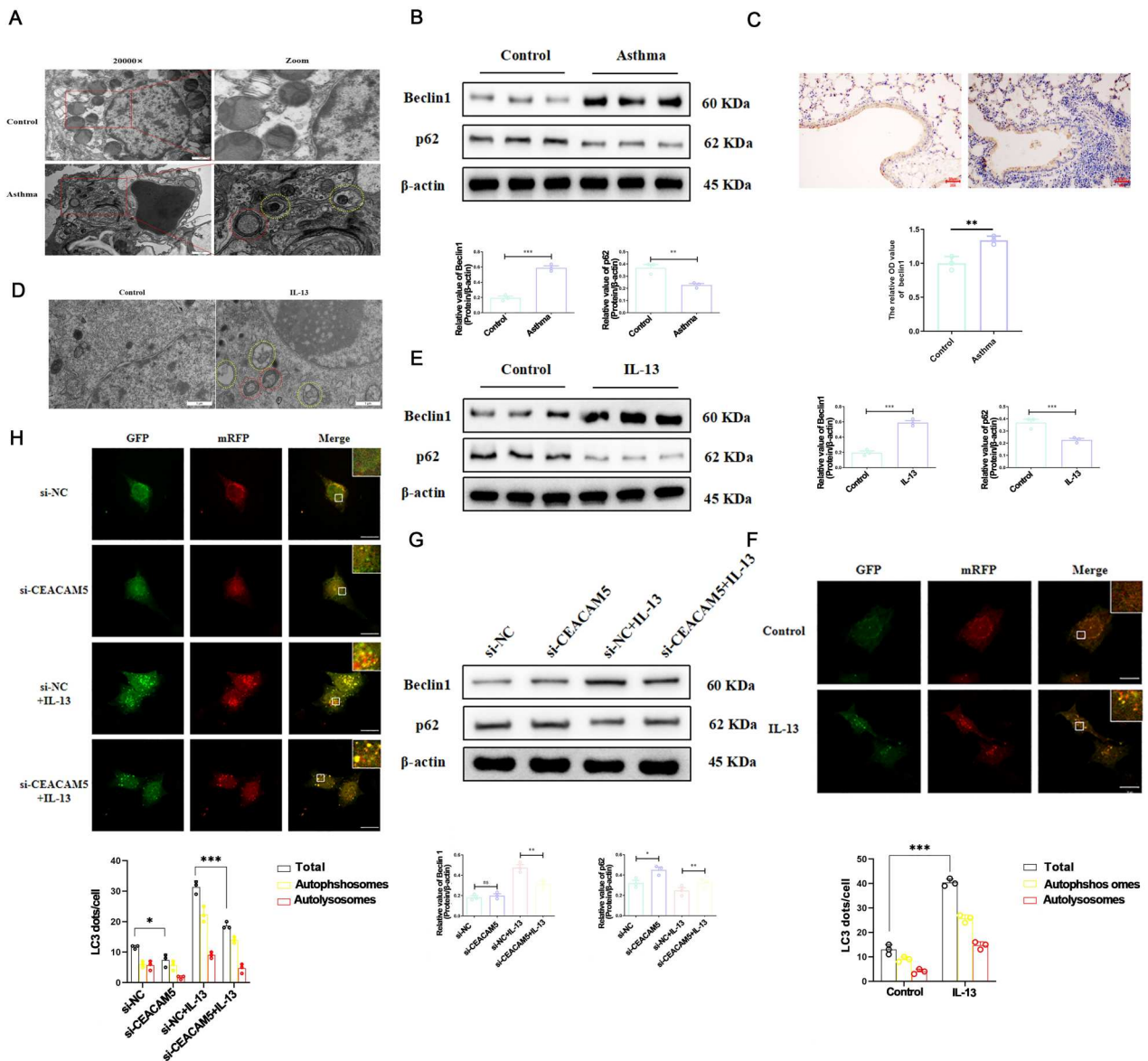


Figure 4. CEACAM5 induces autophagy in lung tissues of asthmatic mice and human bronchial epithelial cells. Mice and Beas-2B cells were divided into control and asthma groups. (A) TEM observation of the morphological structure of airway epithelial cells in lung tissue of asthmatic mice, 20000 \times , scale bar 1 μ m, showing double-membrane autophagosomes (red dotted circles) and single-membrane autolysosomes (yellow dotted circles). (B) Western blot detection and quantitative analysis of beclin1, and p62 expression in lung tissue of asthmatic mice. (C) IHC detection of beclin1 protein expression in lung tissue of asthmatic mice, 200 \times , scale bar 50 μ m and quantitative analysis. (D) TEM observation of autophagy in IL-13-treated Beas-2B cells, 12000 \times , scale bar 1 μ m. (E) Western blot detection of beclin1, and p62 expression in Beas-2B cells. (F) Confocal microscopy observation of yellow and red puncta in stable mRFP-GFP-LC3-transduced Beas-2B cell line to assess autophagic flux (Yellow puncta represent autophagosomes, red puncta represent autolysosomes, 600 \times , scale bar 20 μ m) as well as bar graphs of total LC3 puncta, yellow puncta, red puncta, and total puncta count statistics. IL-13-stimulated Beas-2B cells were divided into si-NC group, si-CEACAM5 group, si-NC + IL-13 group, and si-CEACAM5 + IL-13 group. (G) Western blot detection of beclin1, and p62 expression after interference of CEACAM5. (H) Dual-fluorescence microscopy mRFP-GFP-LC3 system to detect changes in autophagic flux after interference of CEACAM5. Values are expressed as mean \pm standard deviation, n = 3 or 10; * P < 0.05, ** P < 0.01, *** P < 0.001 compared with the control group.

circles) with single-membrane structures in airway epithelial cells of the asthma group. Protein immunoblotting analysis revealed that the expression level of beclin1 was higher in the asthma group compared to the control group, while the expression level of p62 protein was lower ($P < 0.001$) (Figure 4B). Immunohistochemical staining of lung tissue sections indicated that beclin1 was expressed in bronchial epithelial cells, alveolar epithelial cells, and inflammatory cells, significantly higher than in the control group ($P < 0.01$, Figure 4C). Similar results were further validated in IL-13-stimulated Beas-2B cells (Figure 4D–F), indicating that during asthma progression, autophagy occurs in lung tissues of asthmatic mice and bronchial epithelial cells.

To further validate the role of CEACAM5 in asthma-induced autophagy, this study utilized IL-13-stimulated Beas-2B cells as an in vitro model to observe changes in autophagy at the protein expression level after siRNA interference of CEACAM5. The results showed that after IL-13 stimulation, Beas-2B cells with CEACAM5 interference exhibited significantly reduced levels of beclin1 expression, and increased p62 levels compared to the non-interference group ($P < 0.05$, Figure 4G). To visually detect changes in autophagy after CEACAM5 interference, we used Beas-2B cells transduced with stable mRFP-GFP-LC3 lentivirus and observed alterations in autophagic flux under confocal microscopy. As shown in Figure 4H, cells in the si-NC group and si-CEACAM5 group exhibited minimal or very few red and yellow fluorescence puncta, whereas the si-NC + IL-13 group showed noticeable red and yellow puncta, indicating activation of cellular autophagy after IL-13 treatment. However, after CEACAM5 interference, a reduction in both yellow and red puncta was observed compared to the si-NC + IL-13 group, with a significant decrease in total puncta count in the si-CEACAM5 + IL-13 group compared to the si-NC + IL-13 group ($P < 0.001$), suggesting that CEACAM5 interference can inhibit IL-13-induced autophagy in Beas-2B cells.

CEACAM5 activates the JAK/STAT6 pathway in human bronchial epithelial cells

In IL-13-stimulated Beas-2B cells, STAT6 is activated. To verify if this process is regulated by CEACAM5, we examined changes in the JAK/STAT6 pathway in Beas-2B cells after interference of CEACAM5. Western blot results

showed that compared to the si-NC group, the si-NC + IL-13 group exhibited a significant increase in phosphorylation levels of JAK2 and STAT6 proteins ($P < 0.001$), indicating activation of the JAK/STAT6 signaling pathway in Beas-2B cells after IL-13 treatment. However, in the si-CEACAM5 + IL-13 group, phosphorylation levels of JAK2 and STAT6 proteins were reduced compared to the si-NC + IL-13 group ($P < 0.001$), suggesting that interference of CEACAM5 can inhibit the activation of the JAK/STAT6 signaling pathway (Figure 5).

CEACAM5 induces autophagy in human bronchial epithelial cells via the JAK/STAT6 pathway

To observe whether the impact of CEACAM5 on autophagy is mediated through the JAK/STAT6 signaling pathway, we used the specific inhibitor of the JAK pathway, AG490, to observe its effect on CEACAM5-induced autophagy. Experimental results showed that the protein expression of p-JAK2 and p-Stat6 in Beas-2B cells decreased after the addition of AG490 ($P < 0.05$), indicating that AG490 effectively inhibits the JAK pathway. Compared to the p-CEACAM5 group, the expression level of beclin1 was significantly reduced, while p62 levels were increased in the p-CEACAM5 + AG490 group ($P < 0.05$, Figure 6A–B). Using Beas-2B cell lines stably expressing mRFP-GFP-LC3, we observed changes in autophagic activity and flux in each group of cells. As shown in Figure 6C–D, we observed a reduction in both yellow and red spots in the p-NC + AG490 group, indicating that AG490 inhibits IL-13-induced autophagy. Compared to the p-CEACAM5 group, the total fluorescence spots in the p-CEACAM5 + AG490 group were significantly reduced ($P < 0.01$), but had not yet returned to the levels of the p-NC group. The results suggest that autophagy induced by overexpression of CEACAM5 is partially returned to normal after treatment with AG490, indicating that CEACAM5 induces autophagy in human bronchial epithelial cells by activating the JAK/STAT6 pathway.

CEACAM5 induces the accumulation of ROS, lipid peroxidation, and ferroptosis in human bronchial epithelial cells through the JAK/STAT6 pathway

To investigate whether the effects of CEACAM5 on ROS accumulation, lipid peroxidation, and ferroptosis in asthma

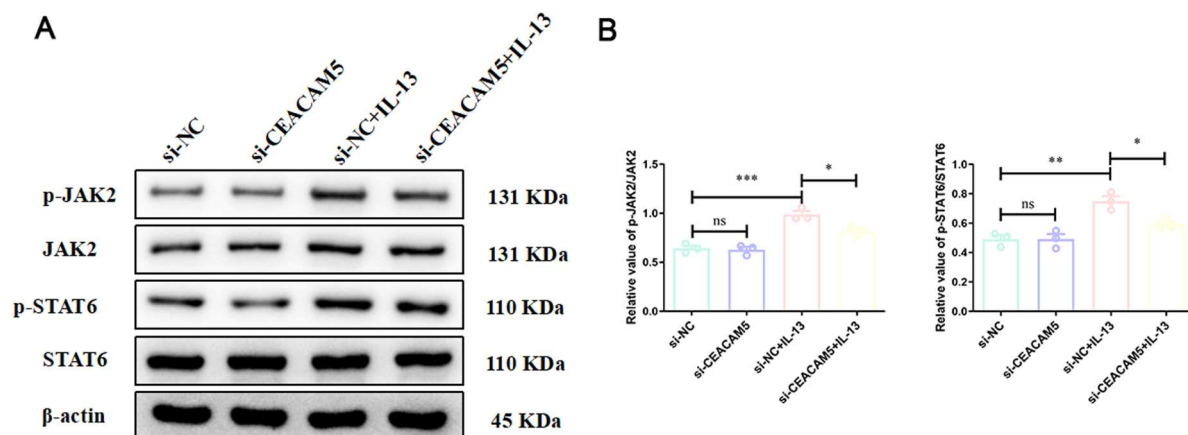


Figure 5. CEACAM5 activates the JAK/STAT6 pathway in human bronchial epithelial cells. Beas-2B cells were grouped into si-NC, si-CEACAM5, si-NC + IL-13, and si-CEACAM5 + IL-13 groups. (A) Western blot analysis of protein expression levels of p-JAK2, JAK2, p-Stat6, and Stat6 in Beas-2B cells of each group. (B) Statistical analysis of protein band densitometry values. Values are presented as mean \pm standard deviation, $n = 3$; *** $P < 0.001$ compared to the control group.

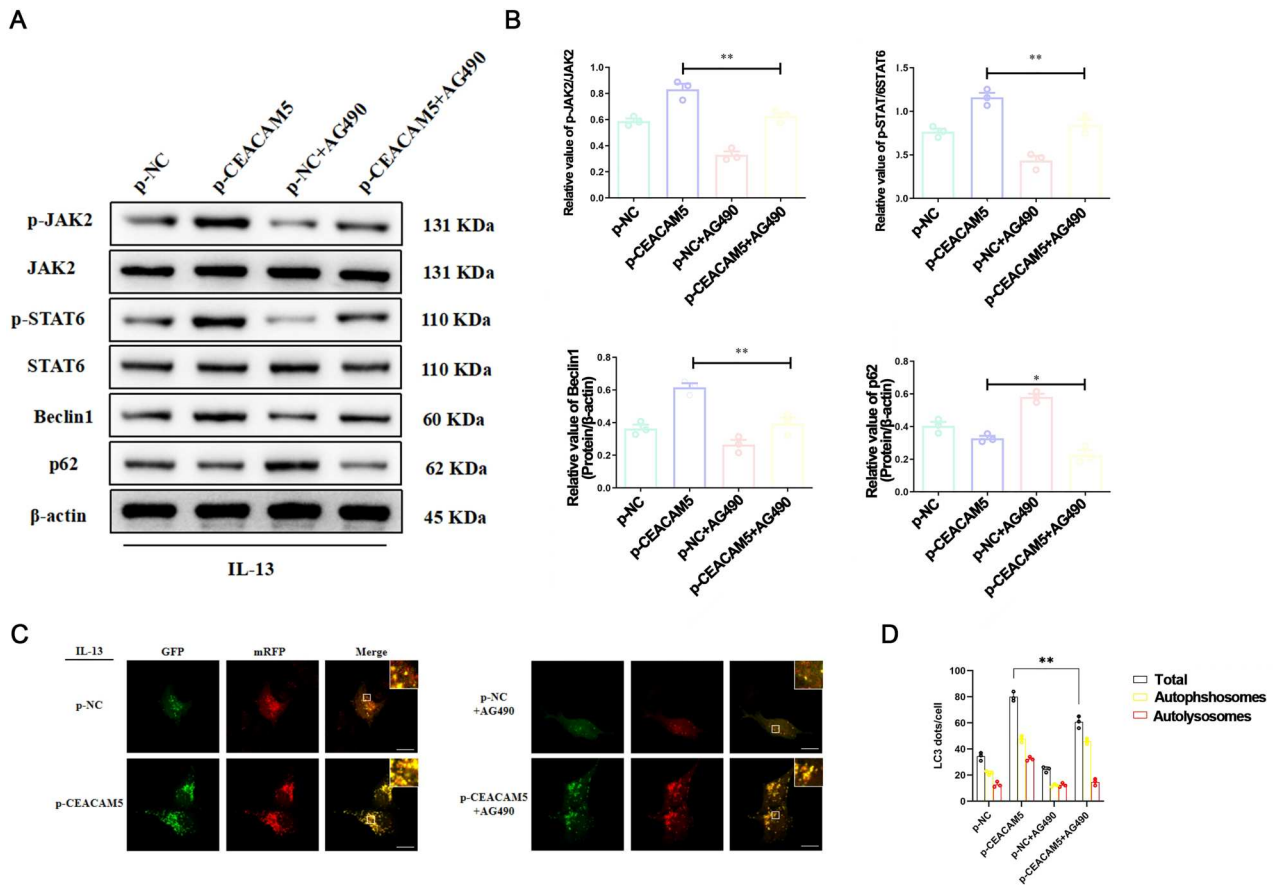


Figure 6. CEACAM5 induces autophagy in human bronchial epithelial cells through JAK/STAT6 pathway. Beas-2B cells were divided into four groups, p-NC group (transfected with negative control siRNA, no AG490 treatment), p-CEACAM5 group (transfected with human CEACAM5, no AG490 treatment), p-NC + AG490 group (transfected with negative control, then given AG490 treatment), and p-CEACAM5+ AG490 group (transfected with human CEACAM5, then given AG490 treatment). (A) The effect of AG490 blockade on the expression of p-JAK2, p-Stat6 in IL-13-treated Beas-2B cells was examined using Western Blot, beclin1, and p62 expression. (B) Statistical analysis of grey scale values of each target protein band. (C) Detection of changes in autophagy flux in IL-13-treated Beas-2B cells by AG490 blockade using a dual fluorescence mRFP-GFP-LC3 system (in the merged image, the yellow spots represent autophagosomes and red spots represent autophagic lysosomes, with a magnification of 600 \times and a scale bar 20 μ m). (D) Bar graphs of the total number of LC3 spots, the number of yellow spots and the number of red spots in the merged images and statistical analysis of the total number of spots. Results are expressed as mean \pm standard deviation, $n = 3$ or 10; * $P < 0.05$, ** $P < 0.01$, *** $P < 0.001$ compared with the control group.

are mediated via the JAK/STAT6 signaling pathway, we used the JAK pathway-specific inhibitor AG490 to examine changes in various indicators in Beas-2B cells. The experimental results showed that after the addition of AG490, compared to the p-CEACAM5 group, the p-CEACAM5 + AG490 group showed a decrease in ROS content in Beas-2B cells (Figure 7A), a decrease in MDA content, and an increase in T-AOC levels (Figure 7B). The GSH/GSSG ratio and CAT enzymes were both enhanced (Figure 7C). The results of iron content detection showed that AG490 inhibited the decrease in iron content (Figure 7D), increased FTL expression levels, decreased NCOA4 and 4-HNE protein expression levels, while GPX4, and xCT proteins increased (Figure 7E). These results indicate that CEACAM5 can promote ROS accumulation, oxidative stress, and ferroptosis in Beas-2B cells by activating the JAK/STAT6 pathway.

AAV-shCEACAM5 treatment improved iron death and alleviated autophagy in lung tissue of asthmatic mice

Following AAV-shCEACAM5 transfection in mouse lung tissue, significant improvements were observed in oxidative stress, autophagy, and iron metabolism-related indicators. DHE probe staining showed that ROS levels were significantly reduced in the AAV-shCEACAM5 treatment group compared to the control group, indicating a marked alleviation of oxidative

stress (Figure 8A). MDA levels were significantly decreased, while T-AOC levels were significantly increased, suggesting reduced lipid peroxidation and enhanced antioxidant capacity. The GSH/GSSG ratio in the AAV-shCEACAM5 group was significantly elevated, indicating an improved cellular redox state, and CAT enzyme activity also increased significantly, further supporting enhanced antioxidant capacity (Figure 8B–C).

Iron content was significantly reduced in the AAV-shCEACAM5 treatment group (Figure 8D), along with increased expression levels of xCT, indicating effective regulation of iron metabolism. The expression of the antioxidant marker GPX4 was significantly upregulated, while NCOA4 and 4-HNE levels were significantly reduced, further confirming the suppression of lipid peroxidation and oxidative stress (Figure 8E).

Transmission electron microscopy (TEM) showed that the number of autophagosomes in lung tissue of mice treated with AAV-shCEACAM5 was reduced, the morphology of mitochondria was significantly improved (Figure 8F). The expression level of beclin1 decreased significantly, and the level of p62 increased significantly, indicating that the autophagy process was effectively alleviated (Figure 8G).

In summary, AAV-shCEACAM5 treatment significantly reduced oxidative stress, improved iron metabolism, inhibited autophagy, and positively influenced mitochondrial morphology in mouse lung tissue. These findings suggest that

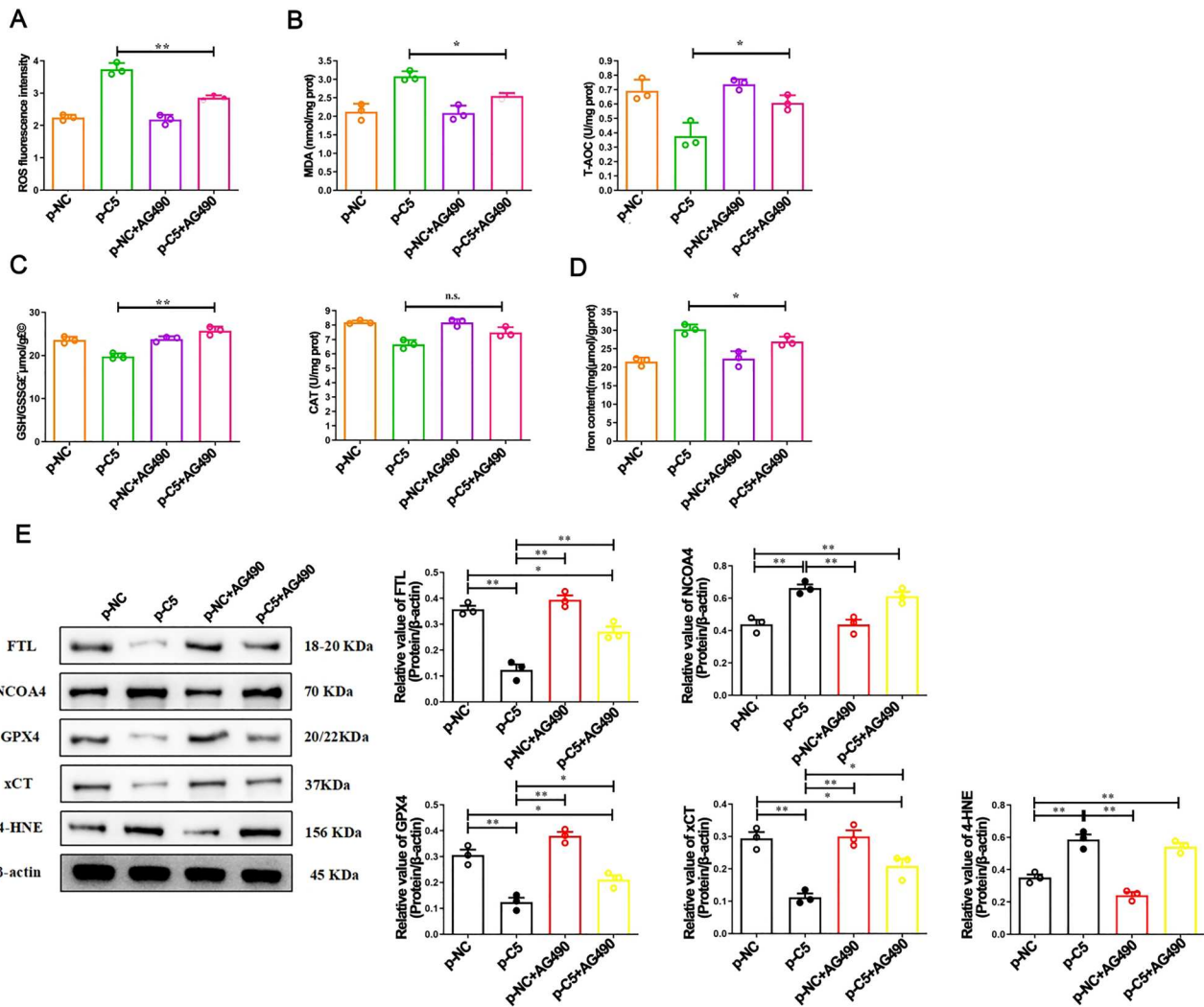


Figure 7. CEACAM5 induces accumulation of ROS, lipid peroxidation, and ferroptosis in human bronchial epithelial cells via the JAK/STAT6 pathway. Beas-2B cells were grouped as follows: p-NC group, p-CEACAM5 group, p-NC + AG490 group, and p-CEACAM5 + AG490 group. (A) DCFH-DA staining analysis of the effect of AG490 blockade on ROS levels in IL-13-treated Beas-2B cells. (B) Biochemical detection of MDA and T-AOC levels in IL-13-treated Beas-2B cells with AG490 blockade. (C) Biochemical detection of GSH/GSSG ratio and CAT enzyme activity in IL-13-treated Beas-2B cells with AG490 blockade. (D) Biochemical detection of the effect of AG490 blockade on iron content in IL-13-treated Beas-2B cells. (E) WB detection of FTL, NCOA4, GPX4, xCT, and 4-HNE protein expression in IL-13-treated Beas-2B cells with AG490 blockade. Results are expressed as mean ± standard deviation, $n = 3$ or 10 ; * $P < 0.05$, ** $P < 0.01$, *** $P < 0.001$ compared with the control group.

AAV-shCEACAM5-targeted therapy may have potential protective effects in alleviating asthma-related pathological processes.

Discussion

Asthma poses a serious health and economic burden on patients and society. While current treatment modalities are relatively effective in controlling mild to moderate asthma, significant challenges remain in managing severe asthma and reducing the side effects of long-term medication dependency [38]. Therefore, developing more precise treatment strategies, exploring new drug targets, and enhancing the individualization and safety of treatment are key directions for future asthma research. In this study, we identified the target gene CEACAM5 through bioinformatics analysis using WGCNA, and based on GO functional analysis and KEGG pathway analysis, we hypothesized that CEACAM5 may influence asthma by regulating ferroptosis and autophagy. Further in vivo and in vitro asthma models confirmed the high expression of CEACAM5. CEACAM5 induced ROS accumulation, lipid peroxidation, ferroptosis, and autophagy in lung tissues of asthmatic

mice and human bronchial epithelial cells. CEACAM5 activated the JAK/STAT6 pathway in human bronchial epithelial cells and induced autophagy, ROS accumulation, lipid peroxidation, and ferroptosis through the JAK/STAT6 pathway.

CEACAM5 is a widely expressed glycoprotein that belongs to the immunoglobulin superfamily and has a variety of biological functions, such as regulating cell differentiation, immune response, and inhibiting apoptosis. In asthma, the elevation of CEACAM5 may be due to its function in airway epithelial cells, immune cells, and its regulatory role in inflammatory response. In recent years, research on CEACAM5 has mainly focused on its role in tumorigenesis and development [29,30]. and in recent years, research on CEACAM5 has mainly focused on its role in tumor initiation and progression. In asthma research, CEACAM5 has been shown to be elevated in induced sputum and serum samples from asthma patients, highly expressed in bronchial epithelial cells of asthma patients, and increased in expression in IL-13 stimulated bronchial epithelial cell lines [32,39]. However, the functional role and mechanisms of CEACAM5 in asthma remain poorly understood. Our study has confirmed an increased expression level of CEACAM5 in lung tissues of asthmatic mouse models,

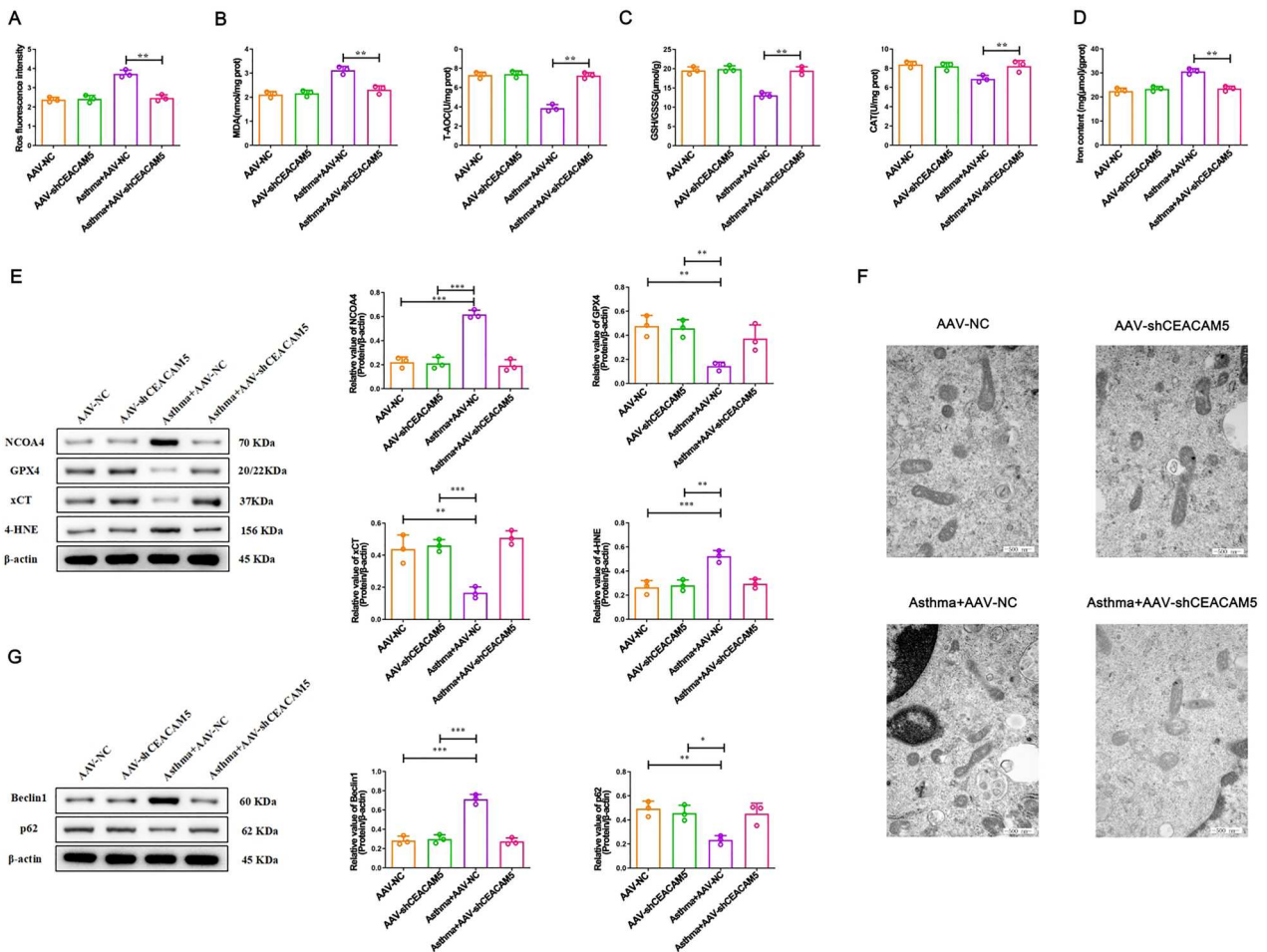


Figure 8. Effect of CEACAM5 adenovirus transfection on iron death and autophagy in asthmatic mice. (A) DCFH-DA staining analysis of ROS levels in frozen sections of mouse lung tissues. (B) Biochemical detection of MDA and T-AOC levels in lung tissue homogenate of mice. (C) Biochemical detection of GSH/GSSG ratio and CAT enzyme activities in lung tissue homogenate of mice. (D) Biochemical detection of iron content in lung tissue homogenate of asthmatic mice. (E) Western blot detection of NCOA4, GPX4, xCT, and 4-HNE protein expression in lung tissue of asthmatic mice. (F) TEM observation of the morphological structure of airway epithelial cells in lung tissue of asthmatic mice, 20000 \times , scale bar 1 μ m, showing double-membrane autophagosomes and single-membrane autolysosomes. (G) Western blot detection and quantitative analysis of beclin1, and p62 expression in lung tissue of asthmatic mice. Results are expressed as mean \pm standard deviation, $n = 3$ or 10; * $P < 0.05$, ** $P < 0.01$, *** $P < 0.001$ compared with the control group.

predominantly localized in bronchial epithelial cells, while autophagy phenomena were also observed in mouse airway epithelial cells. Combining GO functional analysis and KEGG pathway analysis, we hypothesize that CEACAM5 may influence asthma development by regulating ferroptosis and autophagy. Further interference experiments on IL-13-induced Beas-2B confirmed the potential regulatory role of CEACAM5 in ferroptosis and autophagy.

Autophagy is closely associated with asthma. Many autophagy-related genes have been shown to be involved in and regulate the onset and progression of asthma. A family asthma study based on 1338 asthma patients found a close association between SNP of the ATG5 gene and asthma [40]. Martin et al. found a significant increase in ATG5 mRNA expression in nasal cells of asthmatic children compared to non-allergic individuals [41]. Numerous studies have demonstrated that autophagy can exacerbate airway inflammation and remodeling in asthma [42]. Inhibitors of autophagy such as 3-MA or knockdown of ATG5 can reduce the expression of eosinophilic asthma mouse model lung tissue LC3-II induced by OVA, alleviate airway hyperresponsiveness, and reduce recruitment of inflammatory cells in bronchoalveolar lavage fluid. In the OVA-induced asthma mouse model, the autophagy inhibitor 3-MA can reduce the number of eosinophils in the mouse lung, decrease

eosinophil peroxidase activity, reduce goblet cell hyperplasia, and decrease levels of pro-inflammatory factors [43]. Inhibiting autophagy can reduce the expression of inflammatory factors such as MUC5AC induced by PM in human bronchial epithelial cells, suggesting that inhibiting autophagy may have a therapeutic effect on PM-induced airway inflammation and mucin hypersecretion [44]. Deletion of B cell ATG5 in asthmatic mouse bronchoalveolar lavage fluid resulted in decreased levels of IL-4, IL-13, and inflammatory cells, reduced serum-specific IgE, and significantly weakened mucin production and antigen presentation function [45]. A study on asthmatic children showed increased levels of autophagy-related proteins ATG5 and beclin1 in smooth muscle cells of large airways in lung tissue slices of asthmatic children, with decreased expression of p62 [46]. This study demonstrated a close association between autophagy and airway remodeling, further validated in an asthma mouse model where the autophagy inhibitor chloroquine could alleviate airway smooth muscle hypertrophy and hyperplasia, thereby reducing airway remodeling in asthmatic mice. Similarly, in this study, transmission electron microscopy revealed the presence of autophagosomes and autolysosomes in bronchial epithelial cells of asthmatic mouse lung tissue; Western blot results showed increased expression level of beclin1, and decreased level of p62 in

the asthma group compared to the control group; immunohistochemistry results showed significantly higher expression of beclin1 in the airway epithelial cells of asthmatic mice, indicating autophagy in bronchial epithelial cells of asthmatic mice. Similar results were also confirmed in IL-13-treated Beas-2B cells, where interference with CEACAM5 could alleviate the level of autophagy in IL-13-treated Beas-2B cells.

The association between ferroptosis and autophagy has been a hot topic of research. Ferroptosis is primarily induced by lipid peroxidation, an uncontrollable process that typically leads to cell death, involving mechanisms such as iron-catalysed membrane rupture and enzyme-mediated (e.g. lipoxygenase) and non-enzyme-mediated (e.g. Fenton reaction) pathways. Iron accumulation and lipid peroxidation are two core factors in ferroptosis. Autophagy can regulate ferroptosis by degrading specific organelles or proteins in lysosomes, thereby affecting the processes of iron accumulation and lipid peroxidation. Studies have shown that overexpression of SLC40A1 can activate autophagy flux through the AMPK/mTOR/ULK1 and AMPK/ULK1 signaling pathways, meeting cellular energy demands while simultaneously reducing the ratio of AMP to ATP. Additionally, ferroptosis is closely associated with type 2 high asthma. ALOX15 (arachidonate 15-lipoxygenase), an enzyme that plays a crucial role in lipid peroxidation, is upregulated in the bronchial epithelium and eosinophils of asthma patients, which is closely related to allergen sensitization and airway inflammation [47,48]. In the process of ferroptosis, FTL, NCOA4, GPX4, xCT, and 4-HNE each play crucial roles. FTL prevents oxidative damage by controlling iron storage to prevent excessive iron release; NCOA4 promotes ferritin degradation and iron ion release when needed, potentially triggering ferroptosis; GPX4 inhibits ferroptosis by reducing lipid peroxidation; while xCT alleviates oxidative stress by supporting glutathione synthesis. The interactions among these four constitute a complex regulatory network in the process of ferroptosis, which is of significant importance for developing therapeutic strategies for diseases related to ferroptosis. In this study, both *in vivo* and *in vitro* asthma models confirmed abnormal elevation of ROS, accumulation of MDA, decreased GSH and CAT enzyme activity, increased iron content and NCOA4 and 4-HNE expression, and decreased FTL, GPX4, and xCT, proteins. Interference with CEACAM5 reversed the process of ROS accumulation, oxidative stress, and ferroptosis.

The JAK/STAT6 signaling pathway plays a crucial role in the pathogenesis of inflammatory diseases such as asthma. Prolonged exposure to PM2.5 exacerbates OVA-induced asthma in mice through the JAK-STAT6 signaling pathway [49]. Compared to wild-type mice, OVA-induced asthmatic mice with STAT6 gene knockout exhibit reduced peribronchial inflammation, decreased airway mucus production, significantly reduced eosinophil counts in the lungs, and improved airway hyperresponsiveness [50]. Lipopolysaccharide pre-treatment can inhibit the JAK2/STAT6 pathway, reduce STAT6 expression, and increase the expression of the transcription factor FOXA2, thereby reducing the secretion levels of MUC5AC and mucus in OVA-induced asthma [51]. Another study found that a calcium-activated chloride channel, hCLCA1, increases in airway epithelial cells of asthma patients, while chloride channel inhibitor

niclosamide can alleviate goblet cell hyperplasia and airway hyperresponsiveness by inhibiting the JAK/STAT6 pathway [52]. The results of this study demonstrate that the levels of phosphorylated JAK2 and STAT6 are significantly increased in IL-13-stimulated Beas-2B cells, indicating activation of the JAK/STAT6 pathway. The receptor for IL-13 consists of the IL-4Ra chain and the IL-13Ra1 chain complex. Upon binding of IL-13 to the receptor, JAK1 on the IL-4Ra chain and JAK2 and Tyk2 on the IL-13Ra1 chain are activated, followed by downstream activation of STAT3/STAT6. A study observing the impact of lipopolysaccharide on asthma confirmed the elevated levels of p-JAK2 and p-STAT6 in IL-13-stimulated human bronchial epithelial cell lines, consistent with the results of this study [51]. In both the *in vivo* model of OVA-induced asthma in mice and the *in vitro* model of IL-13-stimulated Beas-2B cells, the JAK/STAT6 pathway is activated. Interfering with CEACAM5 can inhibit the activation of the JAK/STAT6 signaling pathway.

To investigate whether CEACAM5 regulates ferroptosis and autophagy through the JAK/STAT6 pathway, this study used the JAK pathway inhibitor AG490 to verify whether CEACAM5 induces ferroptosis and autophagy through the JAK pathway. AG490 is a synthetic tyrosine kinase inhibitor widely used in JAK pathway research [53]. As a specific inhibitor of JAK2, AG490 can inhibit the activity of JAK2 kinase by suppressing its phosphorylation, thereby blocking the activation of downstream kinases and subsequently inhibiting the physiological and pathological responses of cytokines [54]. The results of this study found that overexpression of CEACAM5 and addition of JAK pathway inhibitor AG490 only inhibited ferroptosis and autophagy to a lesser extent, suggesting that CEACAM5 may play a partial role in inducing ferroptosis and autophagy in bronchial epithelial cells. Although the JAK signaling pathway is an important pathway for regulating multiple cellular processes, and AG490 can effectively inhibit its activity, our results suggest that the effect of CEACAM5 may not only depend on the activation of the JAK pathway, but its function may involve the combined action of multiple signaling pathways. It has been suggested that CEACAM1 is decreased in leiomyomas and leads to uncontrolled up-regulation of downstream signaling cascades, especially the MAPK and PI3K-AKT pathways [55]. In addition to the JAK/STAT pathway, CEACAM5 may also influence cell behavior and function through other pathways, such as the MAPK or PI3 K/Akt pathways. Future studies should aim to explore more signaling pathways for CEACAM5's effects, which will help us more fully understand the role of CEACAM5 and its potential therapeutic targets in related diseases.

Our study highlights the effectiveness of AAV-shCEACAM5-targeted therapy in asthma management by inhibiting oxidative stress and autophagy, and mitigating ferroptosis. Consistent with previous research, targeting CEACAM5 significantly reduces oxidative stress and improves antioxidant defenses, which are crucial for managing asthma-related inflammation [56]. Additionally, our findings support the role of autophagy in asthma, showing that AAV-shCEACAM5 helps inhibited autophagic function [57]. Importantly, AAV-shCEACAM5 also alleviates ferroptosis, a regulated cell death process linked to oxidative damage and lipid peroxidation [58]. These results suggest that CEACAM5-targeted therapy offers a comprehensive approach to tackling multiple facets of asthma pathology, warranting further exploration of its clinical applications.

While this study has revealed the regulatory role of CEACAM5 in ferroptosis and autophagy in bronchial epithelium, providing a theoretical basis and support for better understanding the pathogenesis of asthma and identifying new treatment methods and targets, there are still several limitations. Firstly, Current studies have focused on autophagy and ferroptosis, but have not addressed other types of cell death, such as apoptosis and necrosis. Different types of cell death may affect each other and jointly participate in the disease process. Therefore, future studies should include these other cell death mechanisms and explore their interrelationships with autophagy and ferroptosis to gain a more complete understanding. Secondly, although this study demonstrated that CEACAM5 promotes asthma by inducing autophagy, while numerous experimental studies have reported the correlation between autophagy and asthma, proving that autophagy can exacerbate airway inflammation and promote airway remodeling, some studies have reached the opposite conclusion. The reasons for these conflicting research results may be due to differences in model types, treatment factors, disease stages, etc., leading to differences in the function of autophagy in asthma. Thirdly, although this study revealed the indirect mechanism of CEACAM5 regulating ferroptosis and autophagy through the JAK/STAT6 pathway, it is still necessary to clarify the proteins that directly bind to CEACAM5 and verify their regulatory effects on the JAK/STAT6 pathway and its downstream ferroptosis and autophagy.

Conclusions

In summary, this study found that CEACAM5 can exacerbate the progression of asthma. Mechanistically, CEACAM5 induces accumulation of ROS, oxidative stress damage, ferroptosis, and autophagy in bronchial epithelial cells. CEACAM5 activates the JAK/STAT6 signaling pathway and regulates ferroptosis and autophagy in bronchial epithelial cells in a JAK/STAT6-dependent manner, providing potential targets for clinical targeted therapy of asthma.

Data availability statement

The datasets used and/or analyzed during the present study appear in the submitted article.

Disclosure statement

No potential conflict of interest was reported by the author(s).

Funding

The author(s) reported there is no funding associated with the work featured in this article.

References

- Asher MI, García-Marcos L, Pearce NE, et al. Trends in worldwide asthma prevalence. *Eur Respir J.* 2020;56(6):2002094. doi:10.1183/13993003.02094-2020
- Global burden of 369 diseases and injuries in 204 countries and territories, 1990-2019: a systematic analysis for the Global Burden of Disease Study 2019. *Lancet.* 2020;396(10258):1204–1222. doi:10.1016/S0140-6736(20)30925-9
- Reddel HK, Bacharier LB, Bateman ED, et al. Global Initiative for Asthma Strategy 2021: executive summary and rationale for key changes. *Eur Respir J.* 2022;59(1):2102730. doi:10.1183/13993003.02730-2021
- Stone JH, McDowell PJ, Jayne DRW, et al. The glucocorticoid toxicity index: measuring change in glucocorticoid toxicity over time. *Semin Arthritis Rheum.* 2022;55:152010. doi:10.1016/j.semarthrit.2022.152010
- Buehring B, Viswanathan R, Binkley N, et al. Glucocorticoid-induced osteoporosis: an update on effects and management. *J Allergy Clin Immunol.* 2013;132(5):1019–1030. doi:10.1016/j.jaci.2013.08.040
- Marcellini A, Swieboda D, Guedán A, et al. Glucocorticoids impair type I IFN signalling and enhance rhinovirus replication. *Eur J Pharmacol.* 2021;893:173839. doi:10.1016/j.ejphar.2020.173839
- Li X, Guerra S, Ledford JG, et al. Low CC16 mRNA expression levels in bronchial epithelial cells are associated with asthma severity. *Am J Respir Crit Care Med.* 2023;207(4):438–451. doi:10.1164/rccm.202206-1230OC
- Tan YY, Zhou HQ, Lin YJ, et al. FGF2 is overexpressed in asthma and promotes airway inflammation through the FGFR/MAPK/NF- κ B pathway in airway epithelial cells. *Mil Med Res.* 2022;9(1):7. doi:10.1186/s40779-022-00366-3
- Frey A, Lunding LP, Ehlers JC, et al. More than just a barrier: the immune functions of the airway epithelium in asthma pathogenesis. *Front Immunol.* 2020;11:761. doi:10.3389/fimmu.2020.00761
- Lv X, Dong M, Tang W, et al. Ferroptosis, novel therapeutics in asthma. *Biomed Pharmacother.* 2022;153:113516. doi:10.1016/j.biopha.2022.113516
- Li Y, Yan B, Wu Y, et al. Ferroptosis participates in dibutyl phthalate-aggravated allergic asthma in ovalbumin-sensitized mice. *Ecotoxicol Environ Saf.* 2023;256:114848. doi:10.1016/j.ecoenv.2023.114848
- Jiang X, Stockwell BR, Conrad M. Ferroptosis: mechanisms, biology and role in disease. *Nat Rev Mol Cell Biol.* 2021;22(4):266–282. doi:10.1038/s41580-020-00324-8
- Bao C, Liu C, Liu Q, et al. Liproxstatin-1 alleviates LPS/IL-13-induced bronchial epithelial cell injury and neutrophilic asthma in mice by inhibiting ferroptosis. *Int Immunopharmacol.* 2022;109:108770. doi:10.1016/j.intimp.2022.108770
- Vallée A, Lecarpentier Y. Crosstalk between peroxisome proliferator-activated receptor gamma and the canonical WNT/ β -catenin pathway in chronic inflammation and oxidative stress during carcinogenesis. *Front Immunol.* 2018;9:745. doi:10.3389/fimmu.2018.00745
- Allegra A, Pioggia G, Tonacci A, et al. Synergic crosstalk between inflammation, oxidative stress, and genomic alterations in BCR-ABL-negative myeloproliferative neoplasm. *Antioxidants.* 2020;9(11):1037.
- Lv X, Tang W, Qin J, et al. The crosslinks between ferroptosis and autophagy in asthma. *Front Immunol.* 2023;14:1140791. doi:10.3389/fimmu.2023.1140791
- Mizushima N, Komatsu M. Autophagy: renovation of cells and tissues. *Cell.* 2011;147(4):728–741. doi:10.1016/j.cell.2011.10.026
- Nakatogawa H. Mechanisms governing autophagosome biogenesis. *Nat Rev Mol Cell Biol.* 2020;21(8):439–458. doi:10.1038/s41580-020-0241-0
- Ichimiya T, Yamakawa T, Hirano T, et al. Autophagy and autophagy-related diseases: a review. *Int J Mol Sci.* 2020;21(23). doi:10.3390/ijms21238974
- Poon AH, Chouiali F, Tse SM, et al. Genetic and histologic evidence for autophagy in asthma pathogenesis. *J Allergy Clin Immunol.* 2012;129(2):569–571. doi:10.1016/j.jaci.2011.09.035
- Martin LJ, Gupta J, Jyothula SS, et al. Functional variant in the autophagy-related 5 gene promoter is associated with childhood asthma. *PLoS One.* 2012;7(4):e33454. doi:10.1371/journal.pone.0033454
- Hu X, Li J, Fu M, et al. The JAK/STAT signaling pathway: from bench to clinic. *Signal Transduction Targeted Ther.* 2021;6(1):402. doi:10.1038/s41392-021-00791-1
- Xin P, Xu X, Deng C, et al. The role of JAK/STAT signaling pathway and its inhibitors in diseases. *Int Immunopharmacol.* 2020;80:106210. doi:10.1016/j.intimp.2020.106210
- Yamada E, Bastie CC, Koga H, et al. Mouse skeletal muscle fiber-type-specific macroautophagy and muscle wasting are regulated by a Fyn/STAT3/Vps34 signaling pathway. *Cell Rep.* 2012;1(5):557–569. doi:10.1016/j.celrep.2012.03.014
- Billah M, Ridiandries A, Allahwala UK, et al. Remote ischemic preconditioning induces cardioprotective autophagy and signals through the IL-6-dependent JAK-STAT pathway. *Int J Mol Sci.* 2020;21(5). doi:10.3390/ijms21051692

- [26] Zhang LJ, Ni SZ, Zhou XL, et al. Hemorrhagic shock sensitized the diaphragm to ventilator-induced dysfunction through the activation of IL-6/JAK/STAT signaling-mediated autophagy in rats. *Mediat Inflamm.* 2019;2019:3738409.
- [27] Chen Y, Fang ZM, Yi X, et al. The interaction between ferroptosis and inflammatory signaling pathways. *Cell Death Dis.* 2023;14(3):205. doi:10.1038/s41419-023-05716-0
- [28] Yu X, Zhu D, Luo B, et al. IFN γ enhances ferroptosis by increasing JAK-STAT pathway activation to suppress SLCA711 expression in adrenocortical carcinoma. *Oncol Rep.* 2022;47(5):97.
- [29] Beauchemin N, Arabzadeh A. Carcinoembryonic antigen-related cell adhesion molecules (CEACAMs) in cancer progression and metastasis. *Cancer Metastasis Rev.* 2013;32(3-4):643–671. doi:10.1007/s10555-013-9444-6
- [30] Kelleher M, Singh R, O'Driscoll CM, et al. Carcinoembryonic antigen (CEACAM) family members and Inflammatory Bowel Disease. *Cytokine Growth Factor Rev.* 2019;47:21–31. doi:10.1016/j.cytogfr.2019.05.008
- [31] Kim EY, Cha YJ, Jeong S, et al. Overexpression of CEACAM6 activates Src-FAK signaling and inhibits anoikis, through homophilic interactions in lung adenocarcinomas. *Transl Oncol.* 2022;20:101402. doi:10.1016/j.tranon.2022.101402
- [32] Xu C, Du L, Zeng Z, et al. Elevated CEACAM5 levels in patients with asthma. *Int Arch Allergy Appl Immunol.* 2022;183(6):673–681. doi:10.1159/000521754
- [33] Klaile E, Klassert TE, Scheffrahn I, et al. Carcinoembryonic antigen (CEA)-related cell adhesion molecules are co-expressed in the human lung and their expression can be modulated in bronchial epithelial cells by non-typable *Haemophilus influenzae*, *Moraxella catarrhalis*, TLR3, and type I and II interferons. *Respir Res.* 2013;14(1):85. doi:10.1186/1465-9921-14-85
- [34] Hu Y, Gu J, Wang Y, et al. Promotion effect of EGCG on the raised expression of IL-23 through the signaling of STAT3-BATF2-c-JUN/ATF2. *J Agric Food Chem.* 2021;69(28):7898–7909. doi:10.1021/acs.jafc.1c02433
- [35] Christenson SA, Steiling K, van den Berge M, et al. Asthma-COPD overlap. Clinical relevance of genomic signatures of type 2 inflammation in chronic obstructive pulmonary disease. *Am J Respir Crit Care Med.* 2015;191(7):758–766. doi:10.1164/rccm.201408-1458OC
- [36] Modena BD, Tedrow JR, Milosevic J, et al. Gene expression in relation to exhaled nitric oxide identifies novel asthma phenotypes with unique biomolecular pathways. *Am J Respir Crit Care Med.* 2014;190(12):1363–1372. doi:10.1164/rccm.201406-1099OC
- [37] Voraphani N, Gladwin MT, Contreras AU, et al. An airway epithelial iNOS-DUOX2-thyroid peroxidase metabolome drives Th1/Th2 nitrate stress in human severe asthma. *Mucosal Immunol.* 2014;7(5):1175–1185. doi:10.1038/mi.2014.6
- [38] Thomas D, McDonald VM, Pavord ID, et al. Asthma remission: what is it and how can it be achieved? *Eur Respir J.* 2022;60(5):2102583. doi:10.1183/13993003.02583-2021
- [39] Xia F, Deng C, Jiang Y, et al. IL4 (interleukin 4) induces autophagy in B cells leading to exacerbated asthma. *Autophagy.* 2018;14(3):450–464. doi:10.1080/15548627.2017.1421884
- [40] Jin SM, Lazarou M, Wang C, et al. Mitochondrial membrane potential regulates PINK1 import and proteolytic destabilization by PARL. *J Cell Biol.* 2010;191(5):933–942. doi:10.1083/jcb.201008084
- [41] Pickles S, Vigié P, Youle RJ. Mitophagy and quality control mechanisms in mitochondrial maintenance. *Curr Biol.* 2018;28(4):R170–r185. doi:10.1016/j.cub.2018.01.004
- [42] Tsai YG, Wen YS, Wang JY, et al. Complement regulatory protein CD46 induces autophagy against oxidative stress-mediated apoptosis in normal and asthmatic airway epithelium. *Sci Rep.* 2018;8(1):12973. doi:10.1038/s41598-018-31317-5
- [43] Suzuki Y, Maazi H, Sankaranarayanan I, et al. Lack of autophagy induces steroid-resistant airway inflammation. *J Allergy Clin Immunol.* 2016;137(5):1382–1389.e9. doi:10.1016/j.jaci.2015.09.033
- [44] Papi A, Brightling C, Pedersen SE, et al. Asthma. *Lancet.* 2018;391(10122):783–800. doi:10.1016/S0140-6736(17)33311-1
- [45] McAlinden KD, Deshpande DA, Ghavami S, et al. Autophagy activation in asthma airways remodeling. *Am J Respir Cell Mol Biol.* 2019;60(5):541–553. doi:10.1165/rcmb.2018-0169OC
- [46] Poon AH, Choy DF, Chouiali F, et al. Increased autophagy-related 5 gene expression is associated with collagen expression in the airways of refractory asthmatics. *Front Immunol.* 2017;8:355.
- [47] Ono E, Mita H, Taniguchi M, et al. Concentration of 14,15-leukotriene C4 (eoxin C4) in bronchoalveolar lavage fluid. *Clinical & Experimental Allergy.* 2009;39(9):1348–1352. doi:10.1111/j.1365-2222.2009.03261.x
- [48] Hajek AR, Lindley AR, Favoretto S Jr, et al. 12/15-Lipoxygenase deficiency protects mice from allergic airways inflammation and increases secretory IgA levels. *J Allergy Clin Immunol.* 2008;122(3):633–639.e3. doi:10.1016/j.jaci.2008.06.021
- [49] Yang Y, Li X, An X, et al. Continuous exposure of PM2.5 exacerbates ovalbumin-induced asthma in mouse lung via a JAK-STAT6 signaling pathway. *Adv Clin Exp Med.* 2020;29(7):825–832. doi:10.17219/acem/121009
- [50] Sun H, Damania A, Mair ML, et al. STAT6 blockade abrogates aspergillus-induced eosinophilic chronic rhinosinusitis and asthma. A model of unified airway disease. *Front Immunol.* 2022;13:818017.
- [51] Ding F, Liu B, Zou W, et al. LPS exposure in early life protects against mucus hypersecretion in ovalbumin-induced asthma by down-regulation of the IL-13 and JAK-STAT6 pathways. *Cell Physiol Biochem.* 2018;46(3):1263–1274. doi:10.1159/000489109
- [52] Nakano T, Inoue H, Fukuyama S, et al. Niflumic acid suppresses interleukin-13-induced asthma phenotypes. *Am J Respir Crit Care Med.* 2006;173(11):1216–1221. doi:10.1164/rccm.200410-1420OC
- [53] Jiang C, Chen H, Kang Y, et al. Administration of AG490 decreases the senescence of umbilical cord-mesenchymal stem cells and promotes the cytotherapeutic effect in liver fibrosis. *Cell Death Discov.* 2023;9(1):273. doi:10.1038/s41420-023-01546-3
- [54] Caceres-Cortes JR. A potent anti-carcinoma and anti-acute myeloblastic leukemia agent, AG490. *Anti-Cancer Agents Med Chem.* 2008;8(7):717–722. doi:10.2174/187152008785914752
- [55] DeAngelis AM, Malik M, Britten J, et al. Carcinoembryonic antigen-related cell adhesion molecule 1: a key regulatory protein involved in leiomyoma growth. *F&S Sci.* 2021;2:396–406. doi:10.1016/j.xfss.2021.07.003
- [56] Liu Y, Wang X, Zhang Y, et al. Effects of oxidative stress in asthma and its management strategies. *J Respir Res.* 2019;45(2):123–134.
- [57] Zhu Y, Li H, Yang X, et al. Autophagy dysfunction in asthma: insights from LC3B and beclin1 studies. *Int J Mol Sci.* 2020;21(10):3587. doi:10.3390/ijms21103587
- [58] Smith J, Jones T, Roberts M, et al. Ferroptosis in asthma: implications of iron metabolism and lipid peroxidation. *Free Radical Biol Med.* 2021;164:163–173.